responds to various types and levels of stress with apoptosis, cell cycle arrest, senescence, DNA repair, cell metabolism, or autophagy. Moreover, p53 controls *trans*-activation of target genes, which is an essential feature of stress response pathways.[37–39] In other words, p53 activation leads to a complicated network of responses to the various stress signals encountered by cells.[40–44] The mitochondrial respiratory chain produces nitric oxide (NO), which can generate other reactive nitrogen species (RNS) when cells are under hypoxic conditions. Although excess ROS and RNS can engender oxidative and nitrosative stress, moderate-to-low levels of both function in cellular signaling pathways. Especially important are the roles of these mitochondria-generated free radicals in hypoxic signaling pathways, which have important implications for cancer, inflammation, and various other diseases.[25,45] Hypoxic signaling events include vasodilation, modulation of mitochondrial respiration, and cyto-protection following ischemic insult. These phenomena are attributed to the reduction of nitrite anions to nitric oxide if local oxygen levels in tissues decrease,[46] which activates the expression of genes through oxygen-sensitive transcription factors including HIF and NF-κB. Hypoxia-dependent gene expression can have important physiological or pathophysiological consequences for an organism, depending upon the cause of the hypoxic insult.[47] These NO signaling and hypoxia signaling pathways are linked to the p53 pathway,[48] because recent studies have shown that HIF2α inhibition promotes p53-mediated responses by disrupting cellular redox homeostasis, thereby permitting ROS accumulation and DNA damage.[49] Reportedly, hypoxia activates the tumor suppressor protein p53 by up-regulating Sema3E expression.[50]

TGF-β-BMP signaling is involved in developmental morphogenesis and cancer morphogenesis. Morphogens such as those of the TGF-β family inhibit and stimulate basic cell proliferation, respectively, at high and low concentrations. A signaling gradient of declining TGF-β concentration regulates the inhibition and stimulation of cell proliferation.[51] Reactive oxygen species (ROS) can activate TGF-β either directly or indirectly via the activation of proteases. In addition, TGF-β itself induces ROS production as part of its signal-transduction pathway. Pulmonary tissues are vulnerable to the toxic effects of inhaled air. The oxidant pathways are especially relevant in the lung, where TGF-β is known to have a role in tissue repair and connective tissue turnover. In pulmonary fibrosis and renal endothelial cells, TGF-β activation is considered as a hallmark of disease progression.[52–53] In ovarian cancer, over-expression of FOXG1 contributes to TGF-β resistance through inhibition of p21WAF1/CIP1 expression, which is repressed by p53.[54] Tumor necrosis factor (TNF) ligand–receptor signaling occurs because TNF, as a multifunctional cytokine, can induce cell death through receptor-mediated caspase activation and mitochondrial dysfunction by a trigger of oxidative stress induced in cardiovascular disease, neuronal disease, and cancer.[55] Opposing these cell death-promoting signals, binding of TNF receptors can also trigger survival signal activation. A critical balance among various intracellular signaling pathways determines the predominant *in vivo* bioactivity of TNF, as best exemplified by the differential responses of various organs.

A major source of ROS in cells is the mitochondria. Electron leakage from the mitochondrial respiratory chain can react with molecular oxygen, resulting in the formation of the superoxide anion radical, which can subsequently be converted to other ROS. In phagocytes and some cancer cells, ROS are producible through a reaction that is catalyzed by NADPH oxidase complexes. When attackers from the outside, such as environmental stressors, damage mitochondria, electron leakage is also induced; this dysfunction induces severe problems in tissues.[56–59] Mitochondrial dysfunction causes the onset of some diseases.[60–63] Recent evidence has shown that mitochondrial dysfunction is related closely to insulin resistance and metabolic syndrome. The underlying mechanism of mitochondrial dysfunction is very complex, including genetic factors from both the nucleus and mitochondrial genome, with numerous environmental factors also impacting.[64]

Exposure to air pollution, including particles, metals, and other organic compounds as environmental stressors, is associated with pulmonary diseases and cancer. The mechanisms of induced health effects are believed to involve oxidative stress. Oxidative stress mediated by airborne particles and/or fibers might arise from direct generation of ROS from the surfaces of particles and fibers, soluble compounds such as transition metals or organic compounds, and activation of inflammatory cells capable of generating ROS and RNS. Generation of ROS/RNS can cause covalent modifications to DNA directly or they can initiate the formation of genotoxic lipid hydroperoxides. The resulting oxidative DNA damage can engender changed gene expression such as up-regulation of tumor promoters and down-regulation of tumor suppressor genes; the DNA damage might, therefore, be implicated in cancer development. This review describes the important role of free radicals in particle- and fiber-induced cellular damage, the interaction of ROS with target molecules, especially with DNA, and the

modulation of specific genes and transcription factor caused by oxidative stress. Consequently, various environmental stressors cause cellular damage through oxidative stress induction and many signaling pathways. However, what environmental stressor is dominant in which signaling pathway is not always clear. Therefore, identifying gene expression signatures extracted from microarray data can clarify how environmental stressors may damage cells and engender diseases.

Oxidative stress responsiveness in different conditions in rats

From the Gene Expression Omnibus (GEO; <http://www.ncbi.nlm.nih.gov/gds>), 33 independent microarray gene expression data with the same platform GPL341 (Affymetrix) sets in rats were downloaded for this study. All datasets were normalized across all arrays using Z-score transformation methods after combination with respect to probe IDs. The normalized values were filtered with oxidative-related genes listed in this work (see Supplement T2) and then the top 10 genes from up-regulated and down-regulated genes were chosen to analyze gene expression signatures (Table 3). The selected genes were classified using principal component analysis to create gene expression signatures of oxidative stress, and were divided into six groups. Most selected genes could be assigned to gene ontology (GO) categories: DNA repair, oxygen and reactive oxygen species metabolism, and response to stress, but cyclins and cyclin-dependent kinase contained in 'Apoptosis related genes, Cell Cycle Arrest and Checkpoint, Regulation of the Cell Cycle, Regulation of Cell Proliferation, Cell Growth and Differentiation' of 'p53 signaling' and 'TGF-beta signaling' were not observed. Experimental conditions selected from GPL341 datasets in this work were almost all of short-period exposure using *in vivo* and *in vitro* culture systems of rats. It is noteworthy that microarrays capture only transient responses to oxidative stimuli. However, we can predict the underlying mechanism of environmental stressors through oxidative signatures for gene expression. For example, in cluster 1 (GDS964,[65] GDS972,[66] GDS1393,[67] GDS2555,[68] GDS2558,[69]), GPXs, NOS, and NOX were up-regulated, suggesting that environmental stessors in the cluster 1 can activate the NO signaling that leads to inflammation or other cellular damage. Thioredoxin interacting protein, Txnip, was identified as a unique gene in this category. In cluster 2 (GDS696,[70] GDS880,[71] GDS1518,[72] GDS1626,[73] GDS2107,[74] GDS2372,[75] GDS2457,[76] GDS2688[77]), Rad23, Rad50, Rad51c, which are DNA repair and recombination proteins, and the other DNA replication proteins DNA-directed DNA polymerase delta (Pold)1 and Pold3 were classified. This classification suggests that environmental stressors in cluster 2 such as fibronectin, protein restriction, heregulin, kainic acid, hypoxia and ethanol harmed mitochondria or damaged DNA more than the stressors in cluster 1. In cluster 3 (GDS1363,[78] GDS1452[79], GDS1922,[80] GDS2037,[81] GDS2073,[82] GDS2093,[83] GDS 2194,[84], GDS2616,[85] GDS2639,[86] GDS2774,[87] GDS2901,[88] GDM1038,[89]), Gadd45a, Nthl1, Mgmt, Mpp4, Chek1 Cry2, Txnrd1 were observed as up-regulated genes. Since these genes interact with DNA repair and p53 signaling activated, it is possible that environmental stressors in the cluster 3 cause DNA damage and remodeling. In cluster 4 (GDS902,[90] GDS2243,[91] GDS2361,[92]), DNA replication proteins Pinx1 and Slk were detected as unique genes. Especially, STE20-like kinase (Slk) appears to influence cell survival and proliferation. In fact, Slk has been suggested to have a central growth-suppressive role for Mst orthologs, with intriguing possible links to other established tumor suppressors through work in model organisms. Some of the genes in cluster 5 (GDS1027,[93] GDS1273,[94] GDS1959[95]) overlapped with clusters 1 and 3. In cluster 6 (GDS1354,[96] GDS2231[97]), some genes overlapped with clusters 2 and 4. However, Vim was detected as a unique gene in GDS1354, which is an experiment in cirrhotic rats,[96] and up-regulation of this gene was also observed in renal cell carcinoma,[98] cerebral tumors,[99] germ cells, and trophoblastic neoplasms.[100]

Oxidative stress-induce gene expression signatures in human tissues

Among many oxidative responsive pathways, p53 signaling has been studied extensively and has been thought to play a main role in the orchestration of oxidative events in cells. It co-ordinates the cellular responses to a broad range of cellular stress factors. In fact, p53 functions as a node for organizing whether the cell responds to various types and levels of stress with apoptosis, cell cycle arrest, senescence, DNA repair, cell metabolism, or autophagy, as described earlier in this review.[37–39] To control and fine-tune responses to various stress signals encountered by cells, as a transcription factor that both activates and represses a broad range of target genes, p53 demands an exquisitely complicated regulatory network. The

Table 3 The top 10 up-regulated and down-regulated genes in the clusters analyzed

Cluster	GEOID	Environmental stressors (target organ or tissues)	Up-gene	Down-gene
1	GDS964	Methylprednisolone (kidney)	Apoe, Gpx2, Ngb, Nos2, Prdx6, Tmod1, Tnp1, Tpo	Brca2, Cry2, Fen1, Hus1, Ptgs2, Pttg1, Rad50, Srxn1, Xrcc6
	GDS972	Methylprednisolone (liver)	Aass, Atrx, Ncf1, Nqo1, Scd1, Slc41a3, Srd5a2, Tmod1, Tnp1	Chek1, Cry2, Lig1, Mgmt, Pold1, Pold3, Rad50, Rad52, Smc3, Xrcc6
	GDS1393	Streptozotocin (penile cavernosal)	Apc, Cat, Duox2, Gpx2, Gpx6, Gsr, Lpo, Slc38a1, Smc3, Tpo	Atrx, Gpx7, Nos2, Park7, Ptgs2, Scd1, Slc38a4, Slc41a3, Srxn1, Zmynd17
	GDS2555	Trimethyltin (hippocampus)	Apex1, Dnm2, Fancc, Gpx7, Lpo, Mgmt, Park7, Prnp, Txnip, Ucp3	Apc, Apoe, Hbz, Mpp4, Ptgs2, Smc3, Srd5a2, Tnp1, Tpo
	GDS2558	Octreotide (gastric ECL)	Brca1, Brca2, Dnm2, Duox2, Msh2, Nox4, Tmod1, Tpo, Xirp1	Apex1, Atrx, Cry2, Gpx6, Nos2, Slc38a1, Slc38a4, Slk, Tmod1, Tpo
2	GDS696	Fibronectin (ventricular myocytes)	Apoe, Atrx, Chaf1a, Ngb, Rad51c, Smc3, Srxn1, Tpo, Zmynd17	Actb, Atrx, Gsr, Mutyh, Ngb, Prdx6, Rad52, Smc3, Tpo, Txnrd1
	GDS880	Protein restriction (visceral adipose tissue)	Aass, Apc, Gpx6, Gstk1, Ngb, Prnp, Rad51c, Scd1, Tmod1, Tnp1	Brca2, Chaf1a, Lpo, Mutyh, Nos2, Pttg1, Slc38a1, Slc38a4, Tpo, Ung
	GDS1518	Heregulin (ureteric buds)	Dhcr24, Hus1, Ldha, Mif, Park7, Rad1, Rad50, Scd1, Tdg, Ung	Actb, Atrx, Nos2, Nox4, Nqo1, Ptgs1, Rad23a, Srxn1, Txnrd1
	GDS1626	Kainic acid (hippocampi)	Apoe, Brca2, Ncf1, Nox4, Pold1, Rad23a, Rad50, Rad51c, Srd5a2, Tmod1	Chaf1a, Hbz, Lpo, Mb, Pold3, Tnp1, Tpo, Ucp3, Ung, Zmynd17
	GDS2107	Ethanol (pancreas)	Apoe, Atrx, Hbz, Ogg1, Ptgs2, Scd1, Srxn1, Tmod1, Txnrd2, Zmynd17	Cry2, Hus1, Mb, Msh2, Nox4, Nthl1, Prdx6, Rad52, Slk, Srd5a2
	GDS2372	Sulfur dioxide (lung)	Aass, Brca1, Cry2, Hus1, Nos2, Ptgs2, Pttg1, Rad50, Tpo, Zmynd17	Apex1, Brca2, Gpx6, Nos2, Nox4, Rad23a, Rad51c, Srd5a2, Tnp1, Tpo
	GDS2457	Hypoxia (adrenal gland)	Chaf1a, Duox2, Ldha, Ngb, Pold3, Rad23a, Slc41a3, Tpo, Txnrd2	Aass, Apc, Apoe, Atrx, Cry2, Lpo, Nox4, Rad52, Srd5a2, Tnp1
	GDS2688	Methylprednisolone (skeletal muscles)	Aass, Atrx, Hbz, Ngb, Rad1, Scd1, Slc38a5, Tmod1, Tpo, Xirp1	Als2, Atrx, Brca2, Cat, Gsr, Ncf1, Nox4, Nqo1, Slc41a3, Trpc2
3	GDS1363	Forskolin (pheochromocytoma cell)	Aass, Apex1, Brca1, Chek1, Duox2, Gpx2, Hbz, Nxn, Ptgs1, Pttg1	Atrx, Cat, Cygb, Ehd2, Gpx3, Gpx4, Gpx7, Scd1, Sod3, Vim
	GDS1452	N-methyl-N-nitrosourea (mammary tumors)	Cat, Ehd2, Gadd45a, Gstk1, Mgmt, Prdx3, Prdx6, Scd1, Srxn1, Ube2a	Dpagt1, Gab1, Gpx3, Lpo, Mpg, Nxn, Prdx4, Prnp, Rad52, Txnip
	GDS1922	Retinoic X receptor ligand LG100268 (mammary gland)	Brca1, Dnm2, Gpx6, Hbz, Mpp4, Ncf1, Nos2, Slc38a1, Tpo	Aass, Atrx, Chaf1a, Gsr, Idh1, Nox4, Prdx1, Rad23a, Xrcc1, Zmynd17
	GDS2037	Angiopoietin-1 (aortic rings)	Apex1, Dnm2, Mgmt, Ngb, Pold3, Rad50, Slc38a1, Srd5a2, Srxn1, Ucp3	Atrx, Brca2, Chaf1a, Gpx6, Mb, Nox4, Rad23a, Slk, Tpo, Zmynd17
	GDS2073	Isoflurane (basolateral amygdalae)	Brca2, Gpx2, Ift172, Mif, Nos2, Pttg1, Rad1, Rad51c, Tpo, Ung	Atrx, Atrx, Gsr, Nox4, Pold3, Prnp, Ptgs2, Scd1, Smc3, Xrcc6
	GDS2093	Fe-deficiency (jejunum)	Aass, Gadd45a, Gsr, Nqo1, Srxn1, Tdg, Tmod1, Txnrd1, Xrcc1,	Gpx7, Hba-a2, Lpo, Mgmt, Nthl1, Pms2, Rad52, Smc3, Xpc, Xrcc6
	GDS2194	Pregnenolone16alpha-carbonitrile (liver)	Dnm2, Gpx6, Lpo, Nqo1, Prdx5, Ptgs2, Scd1, Srxn1, Tpo, Txnrd1	Aass, Als2, Apoe, Hbz, Nos2, Rad51c, Slc38a5, Srd5a2, Tpo
	GDS2616	Particulate matter (TPM)/l of cigarette smoke (lung)	Aass, Apc, Brca1, Brca2, Cry2, Gpx2, Hus1, Slc38a4, Tpo, Txnrd1	Chaf1a, Mb, Mutyh, Nos2, Pold3, Ptgs2, Rad50, Tmod1, Tnp1, Tpo
	GDS2639	Genistein (mammary epithelial cells)	Atrx, Brca2, Hba-a2, Ngb, Rad23a, Rad52, Smc3, Tpo, Ung, Zmynd17	Apex1, Brca1, Gpx6, Lpo, Pttg1, Slc38a4, Srd5a2, Tnp1, Tpo
	GDS2774	Aging (hippocampi)	Atrx, Ehd2, Gadd45a, Gtf2h1, Mgmt, Ncf1, Nthl1, Ptgs2, Pttg1, Srxn1	Ercc6, Mlh1, Pms2, Rad50, Rad52, Slc38a1, Trpc2, Txnip, Wrnip1, Xpc
	GDS2901	Depolarization. (midbrain)	Apc, Apoe, Atrx, Brca1, Pold3, Ptgs2, Rad23a Slc38a4, Smc3, Zmynd17	Apex1, Atrx, Chaf1a, Gpx2, Hba-a2, Nos2, Pttg1, Srxn1, Tmod1, Tnp1
	GSM1038	Aristolochic acid (kidney)	Apoe, Atrx, Cry2, Ngb, Ppp1r15b, Scd1, Srxn1, Tpo	Apoe, Atrx, Fen1, Gadd45a, Gpx6, Ift172, Pold3, Rad52, Txnip, Zmynd17
4	GDS902	Pyridine activator (ventricular myocytes)	Aass, Chaf1a, Dhcr24, Nthl1, Pinx1, Pold3, Rad52, Scd1, Slc38a1, Xirp1	Apex1, Brca2, Cry2, Gpx6, Hus1, Lpo, Mutyh, Pold1, Rad51c, Tpo
	GDS2243	Re-innervation (tibialis anterior muscles)	Apex1, Atrx, Chek1, Gpx6, Mgmt, Ncf1, Nox4, Pold3, Smc3, Tnp1	Atrx, Brca1, Chaf1a, Lpo, Nthl1, Rad50, Slc41a3, Txnrd2, Ung, Zmynd17
	GDS2361	Hyperinsulinemia (kidney)	Apoe, Chaf1a, Gpx6, Hba-a2, Lpo, Ngb, Ptgs2, Scd1, Slk, Srd5a2	Apc, Atrx, Duox2, Hbz, Mb, Ncf1, Slc38a4, Tmod1, Tnp1, Txnip

Table 3 (cont'd) The top 10 up-regulated and down-regulated genes in the clusters analyzed

Cluster	GEOID	Environmental stressors (target organ or tissues)	Up-gene	Down-gene
5	GDS1027	Sulfur mustard *bis*-(2-chloroethyl) sulfide (lung)	Apoe, Gadd45a, Gpx2, Hba-a2, Mif, Prdx5, Ptgs2, Scd1, Smc3, Srxn1	Apc, Atrx, Dnm2, Duox2, Gab1, Gpx6, Mutyh, Nox4, Srd5a2, Tpo
	GDS1273	Amoxicillin (intestine)	Apc, Apoe, Atrx, Lpo, Mutyh, Slc38a4, Tnp1, Tpo	Apex1, Chaf1a, Cry2, Gpx2, Ngb, Nox4, Scd1, Tpo, Trpc2, Zmynd17
	GDS1959	Ischemia (heart)	Apc, Apoe, Gpx7, Nos2, Nox4, Nxn, Prdx4, Rad52, Scd1, Smc3	Atrx, Brca1, Chaf1a, Hus1, Lpo, Pold1, Prdx5, Rad51c, Slc38a4, Xirp1
6	GDS1354	Carbon tetrachloride (liver)	Chaf1a, Ehd2, Gpx2, Hba-a2, Ncf1, Prnp, Ptgs2, Slc38a4, Vim, Zmynd17	Apoe, Dpagt1, Gab1, Hus1, Nos2, Nxn, Ptgs1, Slk, Trpc2, Txnip
	GDS2231	Dexamethasone (marrow-derived stromal cells)	Apoe, Ehd2, Gpx6, Mgmt, Mpp4, Srd5a2, Tmod1, Tpo	Apex1, Apoe, Chaf1a, Dnm2, Nos2, Rad50, Rad51c, Slk, Smc1a, Smc3

classical model for activation of p53 specifically examines three simple and rate-limiting steps: p53 stabilization induced by ataxia telangiectasia mutated (ATM)/ataxia telangiectasia and Rad3 related (ATR)-mediated phosphorylation, sequence-specific DNA binding, and target gene activation through interaction with the general transcriptional machinery.[29] Recent studies with animal models describe that mouse double minute (Mdm) 2 and MdmX might determine whether a cell responds to p53 activation with growth arrest or apoptosis, but the molecular mechanism of these differential effects remains unknown. In fact, Mdm2 and MdmX can both be recruited to p53 promoter regions. Via a multitude of mechanisms, they can repress transcription of p53 target genes.[101–103] The p53 protein binds sequence-specific regions of DNA of the target gene to process sensing and removal of oxidative damage to nuclear DNA and genetic instability. Furthermore, p53 acts as a transcription factor to regulate the expression of many pro-oxidant and antioxidant genes. A new refined model for p53 activation includes three key steps: (i) p53 stabilization; (ii) anti-repression; and (iii) promoter-specific activation. Among the three steps, most environmental stressors contribute mainly to p53 stabilization and promoter-specific activation. Several reports describe that small weight molecules engender induction of stress-induced genes such as NAD(P)H dehydrogenase, quinone (NQO)1 and NQO2, which stabilize and transiently activate p53 and downstream genes leading to protection against adverse effects of stressors.[104–106]

Therefore, to understand how stress-induced genes are downstream within the p53 pathway, we analyzed gene expression of p53 signaling pathways in array datasets GDS2780[107] and GSE7967[108] that had been obtained from the GEO database. In the GDS2780 study, six heavy metals and three organic compounds that were exposed in liver carcinoma HepG2 cells (Fig. 2A) responded dramatically to gene expression of CHK1, CHK2, Cyclin B Cdc2 p21, p53R2, Cop1-1, and Gadd45. Interestingly, expression levels of p53R2 and Gadd45 responded differently to the heavy metals: p53R2 is likely to associate with mitochondrial DNA and play a critical role in embryogenesis and neurogenesis;[109–113] in contrast, Gadd45 plays a vital role as a cellular stress sensor in the modulation of cell signal transduction in response to stress. Increasing Gadd45 can stabilize p53 activation, leading to cell cycle arrest or procession to apoptosis.[114–116] Consequently, exposure of cultured human cells to heavy metals dramatically altered the gene expression of oxidative-responsive genes. However, in human tissues of the GSE7967 study, the p53 signaling pathway differed from that of heavy metals in the GDS2780 study. Overall, the gene expression signals were weaker than those examined in the GDS2780 study. The GSE7967 study examined cord blood collected at birth from infants whose mothers were exposed or unexposed to arsenic (0.1–68.63 mg/g), showing activation of inflammation and NF-κB signaling in infants born to mothers exposed to arsenic at high concentration. Therefore, after downloading the datasets, we selected four subjects according to blood concentrations of 0.1, 1.76, 9.66, and 68.63 mg/g; then, gene expression of the arsenic (As) exposure-induced responses were visualized in the p53 signaling pathway map (Fig. 2B). The highest concentration subject showed Gadd45, p53-inducible ribonucleotide reductase small subunit 2 (p53R2), spermatogenic leucine zipper 1 (TSP1), cyclinB, Cdc2, Fas, Noxa and ATR that were higher than those of the subject with the low concentration. However, p53 was opposite: high in the low-exposure subject and low in the high-exposure subject, suggesting that the down-regulation of p53 facilitates apoptosis and promotes cell proliferation.

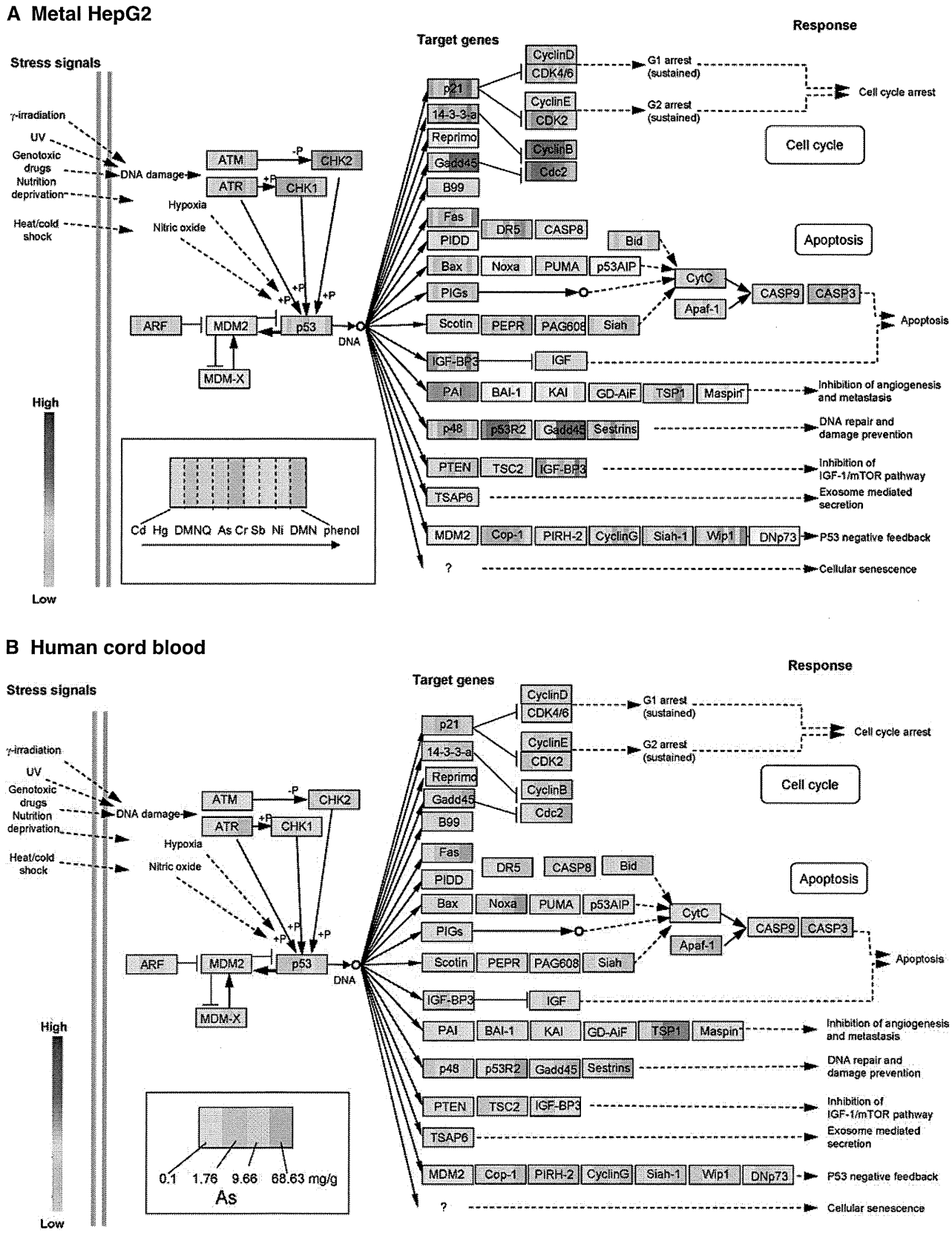

Figure 2 Oxidative gene signature in the p53 signaling pathway pathway in array datasets GDS2780[107](A) and GSE7967[108](B). (A) Heavy metals and organic compounds used in the HepG2 study. Gene expression levels in each box corresponding to each gene symbol are aligned from the left as Cd, Hg, 2,3-dimethoxy-1,4-naphthoquinone (DMNQ), As Cr, Sb, Ni, and DMN, phenol. (B) Human umbilical cord blood. Gene expression levels presented from the left are for 0.1, 1.76, 9.66, and 68.63 mg/g blood arsenic concentration

Previous works described in our study showed that GSS (glutathione synthetase) and PRDX2 (peroxiredoxin 2) regulated TNF receptor-1 associated protein (TRADD), nucleoside diphosphate linked moiety X-type motif 1 (NUDT1), SOD1, and insulin induced gene 1 (INSIG1) in the low-exposure group (mean blood concentration 0.142 μg/g), and that NUDT1 regulated TRADD, TXNRD2, and PRDX2 in the high-exposure group (21.41 μg/g) using the theoretical algorithm for identifying optimal gene expression networks (TAO-Gen), which is a Bayesian network algorithm used to describe gene interaction networks.[17,117–119] In fact, NUDT1 is a DNA repair and recombination protein. The H_2O_2 treatment significantly increased this gene and other oxidative-stress genes involved in cell cycle arrest.[120] Results of our analyses suggest that anti-oxidative stress-related genes play key roles in protection against cellular damage in the low-exposure group, but a DNA damage-related gene was dominant in the high-exposure group, in which cell damage would progress. In addition, TGF-β and TNF signaling were not strongly respondent in this re-analysis, although another paper has described pathways that are shared by oxidatively stressed and early-onset breast cancer associated interactions between TGF-β and TNF signaling.[121] Datasets used in this review are fundamental exposure to environmental stressors in normal tissues and cell lines, Therefore, this discrepancy indicates that gene expression signatures in human clinical tissues or epidemiological studies apparently reflect more inflammation than those of experimental materials, which show acute toxicity in animals after short exposure to oxidants in cell cultures.

Conclusions

Herein, based on recent advances, we surveyed gene expression signatures of environmental stressor-induced oxidative stress and proposed categorical pathways and canonical pathways of oxidative stress in rodent and human systems. Analyses of gene expression signatures in environmental related disease such as neuronal disorders, cancer and diabetes is an important approach in etiology and risk assessment for human health to elucidate the underlying mechanisms of induced health effects. Although we did not survey anti-oxidative stress responses induced by environmental stressors in this review, anti-oxidation systems such as the NRF2-keap1 system should be discussed for association with p53 pathways in an other review. This will take many more genetic and reverse genetic analyses, combined with functional analysis studies. Helped by complementary analyses in environmental stressor or environmental stressor-related disease, we expect soon to see the first attempts to predict influences induced by environmental stressors, taking into account the wealth of experimental data gathered. Although this might uncover interesting feed-forward and feed-back mechanisms, it will take more time to link these signaling interactions to the cell behaviors that control the different aspects of oxygenomics discussed here. It is important to realize that oxygenomics is integral to profiling effects of environmental stressors, which all need to be further classified in this way.

References

1. Gibb S. Toxicity testing in the 21st century: a vision and a strategy. *Reprod Toxicol* 2008; **25**: 136–138.
2. Woods CG, Heuvel JP, Rusyn I. Genomic profiling in nuclear receptor-mediated toxicity. *Toxicol Pathol* 2007; **35**: 474–494.
3. Franco R, Panayiotidis MI. Environmental toxicity, oxidative stress, human disease and the 'black box' of their synergism: how much have we revealed? *Mutat Res* 2009; **674**: 1–2.
4. Hansen JM, Zhang H, Jones DP. Differential oxidation of thioredoxin-1, thioredoxin-2, and glutathione by metal ions. *Free Radic Biol Med* 2006; **40**: 138–145.
5. Valko M, Rhodes CJ, Moncol J, Izakovic M, Mazur M. Free radicals, metals and antioxidants in oxidative stress-induced cancer. *Chem Biol Interact* 2006; **160**: 1–40.
6. Bau DT, Wang TS, Chung CH, Wang AS, Wang AS, Jan KY. Oxidative DNA adducts and DNA-protein cross-links are the major DNA lesions induced by arsenite. *Environ Health Perspect* 2002; **110 (Suppl 5)**: 753–756.
7. Kawai Y, Furuhata A, Toyokuni S, Aratani Y, Uchida K. Formation of acrolein-derived 2'-deoxyadenosine adduct in an iron-induced carcinogenesis model. *J Biol Chem* 2003; **278**: 50346–50354.
8. Chiu HJ, Fischman DA, Hammerling U. Vitamin A depletion causes oxidative stress, mitochondrial dysfunction, and PARP-1-dependent energy deprivation. *FASEB J* 2008; **22**: 3878–3887.
9. Knott L, Hartridge T, Brown NL, Mansell JP, Sandy JR. Homocysteine oxidation and apoptosis: a potential cause of cleft palate. *In Vitro Cell Dev Biol Anim* 2003; **39**: 98–105.
10. Nebert DW, Petersen DD, Fornace Jr AJ. Cellular responses to oxidative stress: the [Ah] gene battery as a paradigm. *Environ Health Perspect* 1990; **88**: 13–25.
11. Cheng Y, Chang LW, Cheng LC, Tsai MH, Lin P. 4-Methoxyestradiol-induced oxidative injuries in human lung epithelial cells. *Toxicol Appl Pharmacol* 2007; **220**: 271–277.
12. Mendrick DL. Genomic and genetic biomarkers of toxicity. *Toxicology* 2008; **245**: 175–181.
13. Luhe A, Suter L, Ruepp S, Singer T, Weiser T, Albertini S. Toxicogenomics in the pharmaceutical industry: hollow promises or real benefit? *Mutat Res* 2005; **575**: 102–115.
14. Wall ME, Dyck PA, Brettin TS. SVDMAN – singular value decomposition analysis of microarray data. *Bioinformatics* 2001; **17**: 566–568.
15. Yeung KY, Ruzzo WL. Principal component analysis for clustering gene expression data. *Bioinformatics* 2001; **17**: 763–774.
16. Portier CJ, Toyoshiba H, Sone H, Parham F, Irwin RD, Boorman GA. Comparative analysis of gene networks at multiple doses and time points in livers of rats exposed to acetaminophen. *Altex* 2006; **23 (Suppl)**: 380–384.

17. Toyoshiba H, Yamanaka T, Sone H *et al.* Gene interaction network suggests dioxin induces a significant linkage between aryl hydrocarbon receptor and retinoic acid receptor beta. *Environ Health Perspect* 2004; **112**: 1217–1224.
18. Bumgarner RE, Yeung KY. Methods for the inference of biological pathways and networks. *Methods Mol Biol* 2009; **541**: 225–245.
19. Huang JC, Babak T, Corson TW *et al.* Using expression profiling data to identify human microRNA targets. *Nat Methods* 2007; **4**: 1045–1049.
20. Li H, Lu L, Manly KF *et al.* Inferring gene transcriptional modulatory relations: a genetical genomics approach. *Hum Mol Genet* 2005; **14**: 1119–1125.
21. Toyokuni S. Molecular mechanisms of oxidative stress-induced carcinogenesis: from epidemiology to oxygenomics. *IUBMB Life* 2008; **60**: 441–447.
22. Kultz D. Molecular and evolutionary basis of the cellular stress response. *Annu Rev Physiol* 2005; **67**: 225–257.
23. Hamilton ML, Van Remmen H, Drake JA *et al.* Does oxidative damage to DNA increase with age? *Proc Natl Acad Sci USA* 2001; **98**: 10469–10474.
24. von Zglinicki T, Saretzki G, Ladhoff J, d'Adda di Fagagna F, Jackson SP. Human cell senescence as a DNA damage response. *Mech Ageing Dev* 2005; **126**: 111–117.
25. Lambeth JD. Nox enzymes, ROS, and chronic disease: an example of antagonistic pleiotropy. *Free Radic Biol Med* 2007; **43**: 332–347.
26. Collado M, Blasco MA, Serrano M. Cellular senescence in cancer and aging. *Cell* 2007; **130**: 223–233.
27. Trachootham D, Alexandre J, Huang P. Targeting cancer cells by ROS-mediated mechanisms: a radical therapeutic approach? *Nat Rev Drug Discov* 2009; **8**: 579–591.
28. Kimbro KS, Simons JW. Hypoxia-inducible factor-1 in human breast and prostate cancer. *Endocr Relat Cancer* 2006; **13**: 739–749.
29. Kruse JP, Gu W. Modes of p53 regulation. *Cell* 2009; **137**: 609–622.
30. Benz CC, Yau C. Ageing, oxidative stress and cancer: paradigms in parallax. *Nat Rev Cancer* 2008; **8**: 875–879.
31. Vousden KH, Ryan KM. p53 and metabolism. *Nat Rev Cancer* 2009; **9**: 691–700.
32. Capri M, Salvioli S, Sevini F *et al.* The genetics of human longevity. *Ann NY Acad Sci* 2006; **1067**: 252–263.
33. Sanchez-Capelo A. Dual role for TGF-beta1 in apoptosis. *Cytokine Growth Factor Rev* 2005; **16**: 15–34.
34. Chalmers L, Kaskel FJ, Bamgbola O. The role of obesity and its bioclinical correlates in the progression of chronic kidney disease. *Adv Chronic Kidney Dis* 2006; **13**: 352–364.
35. Eleuteri E, Magno F, Gnemmi I *et al.* Role of oxidative and nitrosative stress biomarkers in chronic heart failure. *Front Biosci* 2009; **14**: 2230–2237.
36. Albano E. Oxidative mechanisms in the pathogenesis of alcoholic liver disease. *Mol Aspects Med* 2008; **29**: 9–16.
37. Vogelstein B, Lane D, Levine AJ. Surfing the p53 network. *Nature* 2000; **408**: 307–310.
38. Vousden KH, Lane DP. p53 in health and disease. *Nat Rev Mol Cell Biol* 2007; **8**: 275–283.
39. Marchenko ND, Moll UM. The role of ubiquitination in the direct mitochondrial death program of p53. *Cell Cycle* 2007; **6**: 1718–1723.
40. Chao C, Wu Z, Mazur SJ *et al.* Acetylation of mouse p53 at lysine 317 negatively regulates p53 apoptotic activities after DNA damage. *Mol Cell Biol* 2006; **26**: 6859–6869.
41. Chao C, Herr D, Chun J, Xu Y. Ser18 and 23 phosphorylation is required for p53-dependent apoptosis and tumor suppression. *EMBO J* 2006; **25**: 2615–2622.
42. Blattner C, Tobiasch E, Litfen M, Rahmsdorf HJ, Herrlich P. DNA damage induced p53 stabilization: no indication for an involvement of p53 phosphorylation. *Oncogene* 1999; **18**: 1723–1732.
43. Chao C, Hergenhahn M, Kaeser MD *et al.* Cell type- and promoter-specific roles of Ser18 phosphorylation in regulating p53 responses. *J Biol Chem* 2003; **278**: 41028–41033.
44. Brooks CL, Gu W. Ubiquitination, phosphorylation and acetylation: the molecular basis for p53 regulation. *Curr Opin Cell Biol* 2003; **15**: 164–171.
45. Poyton RO, Ball KA, Castello PR. Mitochondrial generation of free radicals and hypoxic signaling. *Trends Endocrinol Metab* 2009; **20**: 332–340.
46. van Faassen EE, Bahrami S, Feelisch M *et al.* Nitrite as regulator of hypoxic signaling in mammalian physiology. *Med Res Rev* 2009; **29**: 683–741.
47. Taylor CT, Cummins EP. The role of NF-kappaB in hypoxia-induced gene expression. *Ann NY Acad Sci* 2009; **1177**: 178–184.
48. Maziere C, Maziere JC. Activation of transcription factors and gene expression by oxidized low-density lipoprotein. *Free Radic Biol Med* 2009; **46**: 127–137.
49. Bertout JA, Majmundar AJ, Gordan JD *et al.* HIF2alpha inhibition promotes p53 pathway activity, tumor cell death, and radiation responses. *Proc Natl Acad Sci USA* 2009; **106**: 14391–14396.
50. Moriya J, Minamino T, Tateno K *et al.* Inhibition of semaphorin as a novel strategy for therapeutic angiogenesis. *Circ Res* 2010; **106**: 391–398.
51. Fosslien E. Cancer morphogenesis: role of mitochondrial failure. *Ann Clin Lab Sci* 2008; **38**: 307–329.
52. Koli K, Myllarniemi M, Keski-Oja J, Kinnula VL. Transforming growth factor-beta activation in the lung: focus on fibrosis and reactive oxygen species. *Antioxid Redox Signal* 2008; **10**: 333–342.
53. Zhang H, Jiang Z, Chang J *et al.* Role of NAD(P)H oxidase in transforming growth factor-beta1-induced monocyte chemoattractant protein-1 and interleukin-6 expression in rat renal tubular epithelial cells. *Nephrology (Carlton)* 2009; **14**: 302–310.
54. Chan DW, Liu VW, To RM *et al.* Overexpression of FOXG1 contributes to TGF-beta resistance through inhibition of p21WAF1/CIP1 expression in ovarian cancer. *Br J Cancer* 2009; **101**: 1433–1443.
55. Tezel G. TNF-alpha signaling in glaucomatous neurodegeneration. *Prog Brain Res* 2008; **173**: 409–421.
56. Aguilera-Aguirre L, Bacsi A, Saavedra-Molina A, Kurosky A, Sur S, Boldogh I. Mitochondrial dysfunction increases allergic airway inflammation. *J Immunol* 2009; **183**: 5379–5387.
57. Bertram KM, Baglole CJ, Phipps RP, Libby RT. Molecular regulation of cigarette smoke induced-oxidative stress in human retinal pigment epithelial cells: implications for age-related macular degeneration. *Am J Physiol* 2009; **297**: C1200–C1210.
58. Lal N, Kumar J, Erdahl WE *et al.* Differential effects of non-steroidal anti-inflammatory drugs on mitochondrial dysfunction during oxidative stress. *Arch Biochem Biophys* 2009; **490**: 1–8.
59. Nelson GM, Ahlborn GJ, Allen JW *et al.* Transcriptional changes associated with reduced spontaneous liver tumor incidence in mice chronically exposed to high dose arsenic. *Toxicology* 2009; **266**: 6–15.
60. Bailey SM. A review of the role of reactive oxygen and nitrogen species in alcohol-induced mitochondrial dysfunction. *Free Radic Res* 2003; **37**: 585–596.
61. Kim GJ, Chandrasekaran K, Morgan WF. Mitochondrial dysfunction, persistently elevated levels of reactive oxygen species and radiation-induced genomic instability: a review. *Mutagenesis* 2006; **21**: 361–367.
62. Protti A, Singer M. Bench-to-bedside review: potential strategies to protect or reverse mitochondrial dysfunction in sepsis-induced organ failure. *Crit Care* 2006; **10**: 228.
63. Shults CW. Mitochondrial dysfunction and possible treatments in Parkinson's disease – a review. *Mitochondrion* 2004; **4**: 641–648.
64. Lee HK, Cho YM, Kwak SH, Lim S, Park KS, Shim EB. Mitochondrial dysfunction and metabolic syndrome-looking for environmental factors. *Biochim Biophys Acta* 2010; **1800**: 282–289.
65. Almon RR, Lai W, DuBois DC, Jusko WJ. Corticosteroid-regulated genes in rat kidney: mining time series array data. *Am J Physiol* 2005; **289**: E870–E882.
66. Jin JY, Almon RR, DuBois DC, Jusko WJ. Modeling of corticosteroid pharmacogenomics in rat liver using gene microarrays. *J Pharmacol Exp Ther* 2003; **307**: 93–109.
67. Sullivan CJ, Teal TH, Luttrell IP, Tran KB, Peters MA, Wessells H. Microarray analysis reveals novel gene expression changes associated with erectile dysfunction in diabetic rats. *Physiol Genomics* 2005; **23**: 192–205.
68. Lattanzi W, Bernardini C, Gangitano C, Michetti F. Hypoxia-like transcriptional activation in TMT-induced degeneration: microarray expression analysis on PC12 cells. *J Neurochem* 2007; **100**: 1688–1702.
69. Erlandsen SE, Fykse V, Waldum HL, Sandvik AK. Octreotide induces apoptosis in the oxyntic mucosa. *Mol Cell Endocrinol* 2007; 264: 188–196.
70. Chen H, Huang XN, Stewart AF, Sepulveda JL. Gene expression changes associated with fibronectin-induced cardiac myocyte hypertrophy. *Physiol Genomics* 2004; **18**: 273–283.

71. Guan H, Arany E, van Beek JP *et al.* Adipose tissue gene expression profiling reveals distinct molecular pathways that define visceral adiposity in offspring of maternal protein-restricted rats. *Am J Physiol* 2005; **288**: E663–E673.
72. Sakurai H, Bush KT, Nigam SK. Heregulin induces glial cell line-derived neurotrophic growth factor-independent, non-branching growth and differentiation of ureteric bud epithelia. *J Biol Chem* 2005; **280**: 42181–42187.
73. Koh S, Chung H, Xia H, Mahadevia A, Song Y. Environmental enrichment reverses the impaired exploratory behavior and altered gene expression induced by early-life seizures. *J Child Neurol* 2005; **20**: 796–802.
74. Kubisch CH, Gukovsky I, Lugea A *et al.* Long-term ethanol consumption alters pancreatic gene expression in rats: a possible connection to pancreatic injury. *Pancreas* 2006; **33**: 68–76.
75. Kodavanti UP, Schladweiler MC, Ledbetter AD *et al.* The spontaneously hypertensive rat: an experimental model of sulfur dioxide-induced airways disease. *Toxicol Sci* 2006; **94**: 193–205.
76. Bruder ED, Lee JJ, Widmaier EP, Raff H. Microarray and real-time PCR analysis of adrenal gland gene expression in the 7-day-old rat: effects of hypoxia from birth. *Physiol Genomics* 2007; **29**: 193–200.
77. Almon RR, DuBois DC, Yao Z, Hoffman EP, Ghimbovschi S, Jusko WJ. Microarray analysis of the temporal response of skeletal muscle to methylprednisolone: comparative analysis of two dosing regimens. *Physiol Genomics* 2007; **30**: 282–299.
78. Chan MM, Lu X, Merchant FM, Iglehart JD, Miron PL. Gene expression profiling of NMU-induced rat mammary tumors: cross species comparison with human breast cancer. *Carcinogenesis* 2005; **26**: 1343–1353.
79. Kendziorski C, Irizarry RA, Chen KS, Haag JD, Gould MN. On the utility of pooling biological samples in microarray experiments. *Proc Natl Acad Sci USA*. 2005; **102**: 4252-4257.
80. Aplin AC, Gelati M, Fogel E, Carnevale E, Nicosia RF. Angiopoietin-1 and vascular endothelial growth factor induce expression of inflammatory cytokines before angiogenesis. *Physiol Genomics* 2006; **27**: 20–28.
81. Rampil IJ, Moller DH, Bell AH. Isoflurane modulates genomic expression in rat amygdala. *Anesth Analg* 2006; **102**: 1431–1438.
82. Collins JF. Gene chip analyses reveal differential genetic responses to iron deficiency in rat duodenum and jejunum. *Biol Res* 2006; **39**: 25–37.
83. Guzelian J, Barwick JL, Hunter L, Phang TL, Quattrochi LC, Guzelian PS. Identification of genes controlled by the pregnane X receptor by microarray analysis of mRNAs from pregnenolone 16alpha-carbonitrile-treated rats. *Toxicol Sci* 2006; **94**: 379–387.
84. Gebel S, Gerstmayer B, Kuhl P, Borlak J, Meurrens K, Muller T. The kinetics of transcriptomic changes induced by cigarette smoke in rat lungs reveals a specific program of defense, inflammation, and circadian clock gene expression. *Toxicol Sci* 2006; **93**: 422–431.
85. Su Y, Simmen FA, Xiao R, Simmen RC. Expression profiling of rat mammary epithelial cells reveals candidate signaling pathways in dietary protection from mammary tumors. *Physiol Genomics* 2007; **30**: 8–16.
86. Rowe WB, Blalock EM, Chen KC *et al.* Hippocampal expression analyses reveal selective association of immediate-early, neuroenergetic, and myelinogenic pathways with cognitive impairment in aged rats. *J Neurosci* 2007; **27**: 3098–3110.
87. Volpicelli F, Caiazzo M, Greco D *et al.* Bdnf gene is a downstream target of Nurr1 transcription factor in rat midbrain neurons in vitro. *J Neurochem* 2007; **102**: 441–453.
88. Stemmer K, Ellinger-Ziegelbauer H, Ahr HJ, Dietrich DR. Carcinogen-specific gene expression profiles in short-term treated Eker and wild-type rats indicative of pathways involved in renal tumorigenesis. *Cancer Res* 2007; **67**: 4052–4068.
89. Impey S, McCorkle SR, Cha-Molstad H *et al.* Defining the CREB regulon: a genome-wide analysis of transcription factor regulatory regions. *Cell* 2004; **119**: 1041–1054.
90. Bush EW, Hood DB, Papst PJ *et al.* Canonical transient receptor potential channels promote cardiomyocyte hypertrophy through activation of calcineurin signaling. *J Biol Chem* 2006; **281**: 33487–33496.
91. Zhou Z, Cornelius CP, Eichner M, Bornemann A. Reinnervation-induced alterations in rat skeletal muscle. *Neurobiol Dis* 2006; **23**: 595–602.
92. Bursztyn M, Gross ML, Goltser-Dubner T, et al. Adult hypertension in intrauterine growth-restricted offspring of hyperinsulinemic rats: evidence of subtle renal damage. *Hypertension* 2006; **48**: 717–723.
93. Thomas H, Senkel S, Erdmann S *et al.* Pattern of genes influenced by conditional expression of the transcription factors HNF6, HNF4alpha and HNF1beta in a pancreatic beta-cell line. *Nucleic Acids Res* 2004; **32**: e150.
94. Schumann A, Nutten S, Donnicola D *et al.* Neonatal antibiotic treatment alters gastrointestinal tract developmental gene expression and intestinal barrier transcriptome. *Physiol Genomics* 2005; **23**: 235–245.
95. Roy S, Khanna S, Kuhn DE *et al.* Transcriptome analysis of the ischemia-reperfused remodeling myocardium: temporal changes in inflammation and extracellular matrix. *Physiol Genomics*. 2006; **25**: 364–374.
96. Tugues S, Morales-Ruiz M, Fernandez-Varo G *et al.* Microarray analysis of endothelial differentially expressed genes in liver of cirrhotic rats. *Gastroenterology* 2005; **129**: 1686–1695.
97. Akavia UD, Shur I, Rechavi G, Benayahu D. Transcriptional profiling of mesenchymal stromal cells from young and old rats in response to Dexamethasone. *BMC Genomics* 2006; **7**: 95.
98. Zhou M, Roma A, Magi-Galluzzi C. The usefulness of immunohistochemical markers in the differential diagnosis of renal neoplasms. *Clin Lab Med* 2005; **25**: 247–257.
99. Schiffer D, Giordana MT, Mauro A, Migheli A, Germano I, Giaccone G. Immunohistochemical demonstration of vimentin in human cerebral tumors. *Acta Neuropathol* 1986; **70**: 209–219.
100. Niehans GA, Manivel JC, Copland GT, Scheithauer BW, Wick MR. Immunohistochemistry of germ cell and trophoblastic neoplasms. *Cancer* 1988; **62**: 1113–1123.
101. Iwakuma T, Lozano G. Crippling p53 activities via knock-in mutations in mouse models. *Oncogene* 2007; **26**: 2177–2184.
102. Marine JC, Jochemsen AG. Mdmx as an essential regulator of p53 activity. *Biochem Biophys Res Commun* 2005; **331**: 750–760.
103. Tang Y, Zhao W, Chen Y, Zhao Y, Gu W. Acetylation is indispensable for p53 activation. *Cell* 2008; **133**: 612–626.
104. Gong X, Kole L, Iskander K, Jaiswal AK. NRH:quinone oxidoreductase 2 and NAD(P)H:quinone oxidoreductase 1 protect tumor suppressor p53 against 20s proteasomal degradation leading to stabilization and activation of p53. *Cancer Res* 2007; **67**: 5380–5388.
105. Lai Z, Yang T, Kim YB *et al.* Differentiation of Hdm2-mediated p53 ubiquitination and Hdm2 autoubiquitination activity by small molecular weight inhibitors. *Proc Natl Acad Sci USA* 2002; **99**: 14734–14739.
106. Wang W, Ho WC, Dicker DT *et al.* Acridine derivatives activate p53 and induce tumor cell death through Bax. *Cancer Biol Ther* 2005; **4**: 893–898.
107. Kawata K, Yokoo H, Shimazaki R, Okabe S. Classification of heavy-metal toxicity by human DNA microarray analysis. *Environ Sci Technol* 2007; **41**: 3769–3774.
108. Fry RC, Navasumrit P, Valiathan C *et al.* Activation of inflammation/NF-kappaB signaling in infants born to arsenic-exposed mothers. *PLoS Genet* 2007; **3**: e207.
109. Chang L, Zhou B, Hu S *et al.* ATM-mediated serine 72 phosphorylation stabilizes ribonucleotide reductase small subunit p53R2 protein against MDM2 to DNA damage. *Proc Natl Acad Sci USA* 2008; **105**: 18519–18524.
110. Kollberg G, Darin N, Benan K *et al.* A novel homozygous RRM2B missense mutation in association with severe mtDNA depletion. *Neuromuscul Disord.* 2009; **19**: 147–150.
111. Liu X, Xue L, Yen Y. Redox property of ribonucleotide reductase small subunit M2 and p53R2. *Methods Mol Biol* 2008; **477**: 195–206.
112. Spinazzola A, Invernizzi F, Carrara F *et al.* Clinical and molecular features of mitochondrial DNA depletion syndromes. *J Inherit Metab Dis* 2009; **32**: 143–158.
113. Tyynismaa H, Suomalainen A. Mouse models of mitochondrial DNA defects and their relevance for human disease. *EMBO Rep* 2009; **10**: 137–143.
114. Ceryak S, Zingariello C, O'Brien T, Patierno SR. Induction of pro-apoptotic and cell cycle-inhibiting genes in chromium (VI)-treated human lung fibroblasts: lack of effect of ERK. *Mol Cell Biochem* 2004; **255**: 139–149.
115. Fanzo JC, Reaves SK, Cui L *et al.* Zinc status affects p53, gadd45, and c-fos expression and caspase-3 activity in human bronchial epithelial cells. *Am J Physiol* 2001; **281**: C751–C757.

116. Shih RS, Wong SH, Schoene NW, Lei KY. Suppression of Gadd45 alleviates the G2/M blockage and the enhanced phosphorylation of p53 and p38 in zinc supplemented normal human bronchial epithelial cells. *Exp Biol Med (Maywood)* 2008; **233**: 317–327.
117. Toyoshiba H, Sone H, Yamanaka T *et al.* Gene interaction network analysis suggests differences between high and low doses of acetaminophen. *Toxicol Appl Pharmacol* 2006; **215**: 306–316.
118. Yamanaka T, Toyoshiba H, Sone H, Parham FM, Portier CJ. The TAO-Gen algorithm for identifying gene interaction networks with application to SOS repair in *E. coli*. *Environ Health Perspect* 2004; **112**: 1614–1621.
119. Sone H, Imanishi S, Akanuma H *et al.* Gene expression signatures of environmental chemicals in cancer and in developmental disorders. In: Zhao BDM, Cadeans E. (eds) *The roles of free radicals in biology and medicine*. Beijing: Medimond, 2009; 45–52.
120. Chua PJ, Yip GW, Bay BH. Cell cycle arrest induced by hydrogen peroxide is associated with modulation of oxidative stress related genes in breast cancer cells. *Exp Biol Med (Maywood)* 2009; **234**: 1086–1094.
121. Feng XD, Huang SG, Shou JY *et al.* Analysis of pathway activity in primary tumors and NCI60 cell lines using gene expression profiling data. *Genomics Proteomics Bioinformatics* 2007; **5**: 15–24.

SUPPLEMENTAL MATERIALS
Supplement T1 – oxidative stress pathways

Categorical pathways Canonical pathway (orthology)	Gene name
Reactive oxygen species (ROS) metabolism and antioxidant defenses	
Glutathione peroxidases (GPx)	GPX1, GPX2, GPX3, GPX4, GPX5, GPX6, GPX7, GSTZ1
Peroxiredoxins (TPx)	PRDX1, PRDX2, PRDX3, PRDX4, PRDX5, PRDX6
Other peroxidases	CAT, CSDE1, CYGB, DUOX1, DUOX2, EPX, GPR156, LPO, MGST3, MPO, PIP3-E, PTGS1, PTGS2, PXDN, PXDNL, TPO, TTN
Other antioxidants	ALB, APOE, GSR, MT3, SELS, SRXN1, TXNDC2, TXNRD1, TXNRD2
Superoxide dismutases (SOD)	SOD1, SOD2, SOD3
Other genes involved in superoxide metabolism	ALOX12, CCS, CYBA, DUOX1, DUOX2, GTF2I, MT3, NCF1, NCF2, NOS2A, NOX5, PREX1, PRG3
Genes involved in ROS metabolism	AOX1, BNIP3, EPHX2, MPV17, SFTPD
Oxidative stress responsive genes	ANGPTL7, ATOX1, CAT, CCL5, CSDE1, DGKK, DHCR24, DUSP1, EPX, FOXM1, GLRX2, GPR156,GSS, KRT1, LPO, MBL2, MPO, MSRA, MTL5, NME5, NUDT1, OXR1, OXSR1, PDLIM1, PIP3-E, PNKP, PRDX2, PRDX5, PRDX6, PRNP, RNF7, SCARA3, SELS, SEPP1, SGK2, SIRT2, SRXN1, STK25, TPO, TTN
p53 signaling pathway	
Induction of apoptosis	BAX, BID, CDKN1A, CRADD, EI24, FADD, FASLG (TNFSF6), FOXO3, PCBP4, PRKCA, TNFRSF10B, TP53, TP73, TP73L
Anti-apoptosis	BCL2, BCL2A1, BIRC5, CASP2, HDAC1, IGF1R, MCL1, NFKB1, RELA, TNF, TNFRSF10
Other apoptosis genes	APAF1, BRCA1, CASP9, E2F1, GADD45A, GML, LRDD, P53AIP1, SIAH1, SIRT1, TP53BP2, TRAF2
Cell cycle arrest	CDKN1A, CDKN2A, CHEK1, CHEK2, GADD45A, GML, MYC, PCAF, PCBP4, RPRM, SESN1, SESN2
Cell cycle checkpoint	ATR, BRCA1, CCNE2, CCNG2, CDKN2A, RB1, TP53
Negative regulation of the cell cycle	BAX, BRCA1, CDKN2A, MSH2, NF1, PTEN, RB1, TP53, TP73, TP73L, TSC1, WT1
Regulation of the cell cycle	BRCA2, CDC2, CDC25A, CDK4, E2F1, E2F3, HK2, IGF1R, KRAS, PPM1D, PRKCA, STAT1, TADA3L, TP53BP2
Other cell cycle genes	BIRC5, CCNH, CCNB2, ESR1, MLH1, PCNA, PRC1
Negative regulation of cell proliferation	BAI1, BCL2, BTG2, CDKN1A, CDKN2A, CHEK1, GML, IFNB1, IL6, MDM2, MDM4, NF1, PCAF, PPM1D, SESN1
Positive regulation of cell proliferation	IGF1R, IL6
Cell Proliferation	BRCA1, CDC25A, CDC25C, CDK4, E2F1, MYC, PCNA, PRKCA
Cell growth and differentiation	ESR1, MCL1, MYOD1
Other genes related to cell growth, proliferation, and differentiation	EGR1, FOXO3A, JUN, KRAS, PTTG1
DNA repair genes	ATM, ATR, BRCA1, BTG2, CCNH, DNMT1, GADD45A, MSH2, PCNA, PTTG1, TP53, XRCC5
Human nitric oxide signaling pathway PCR array	
Genes with nitric-oxide synthase or oxidoreductase activity	NOS1, NOS2A, NOS3, NQO1
Positive regulators of nitric oxide biosynthesis	HSP90AB1 (HSPCB), INS
Negative regulators of nitric oxide biosynthesis	DNCL1, GLA, IL10
Other genes involved in NO biosynthesis	AKT1, ARG2, DDAH2, DNCL1, EGFR, GCH1, GCHFR

Genes induced by NO	CDKN1A, IL8, JUN, VEGFA
Genes suppressed by NO	CCNA1, MYB, TROAP
Genes involved in NO signaling pathway	CAMK1, DLG4, GRIN2D, NOS1, PPP3CA, PRKAR1B, PRKCA
Genes involved in superoxide release	ALOX12, DUOX1, DUOX2, NOX5, PRG3
Genes with oxidoreductase activity	ALOX12, CYBA, DUOX1, DUOX2, NOS2A, NOX5, SOD1, SOD2, SOD3
Genes with peroxidase activity	DUOX1, DUOX2
Genes with superoxide dismutase activity	SOD2
Other genes involved in superoxide metabolism	CCS, NCF1, NCF2, PREX1
Anti-apoptosis genes	MPO, MTL5, NME5, PRDX2, RNF7
Genes with antioxidant activity	APOE, MT3, SELS, SOD1, SOD3, SRXN1 (C20orf139)
Genes with glutathione peroxidase activity	GPX1, GPX2, GPX3, GPX4, GPX5, GPX6, LOC493869
Genes with oxidoreductase activity	CAT, EPX, GPX1, GPX2, GPX3, GPX4, GPX5, GPX6, LPO, MPO, MSRA, PRDX2, PRDX6, SOD1, SOD2, SRXN1(C20orf139), TPO, TXNRD2
Genes with peroxidase activity	CYGB, EPX, GPR156, LPO, MPO, PRDX2, PRDX5, PRDX6, TPO, TTN, UNR
Transcription regulators	FOXM1, GLRX2, SCRT2, SIRT2, SOD2, UNR
Other genes involved in oxidative stress	ATOX1, DUSP1, GSS, KRT1, MBL2, NUDT1, OXR1, PNKP, PRNP, SCARA3, SEPP1, SGK2
DNA damage signaling	
Apoptosis	ABL1, BRCA1, CIDEA, GADD45A, GADD45G, GML, IHPK3, PCBP4, AIFM1 (PDCD8), PPP1R15A, RAD21, TP53, TP73
Cell cycle arrest	CHEK1, CHEK2, DDIT3 (CHOP), GADD45A, GML, GTSE1, HUS1, MAP2K6, MAPK12, PCBP4, PPP1R15A, RAD17, RAD9A, SESN1, ZAK
Cell cycle checkpoint	ATR, BRCA1, FANCG, NBN (NBS1), RAD1, RBBP8, SMC1A (SMC1L1), TP53
Damaged DNA binding	ANKRD17, BRCA1, DDB1, DMC1, ERCC1, FANCG, FEN1, MPG, MSH2, MSH3, N4BP2, NBN (NBS1), OGG1, PMS2L3 (PMS2L9), PNKP, RAD1, RAD18, RAD51, RAD51L1, REV1 (REV1L), SEMA4A, XPA, XPC, XRCC1, XRCC2, XRCC3
Base-excision repair	APEX1, MBD4, MPG, MUTYH, NTHL1, OGG1, UNG
Double-strand break repair	CIB1, FEN1, XRCC6 (G22P1), XRCC6BP1 (KUB3), MRE11A, NBN (NBS1), PRKDC, RAD21, RAD50
Mismatch Repair	ABL1, ANKRD17, EXO1, MLH1, MLH3, MSH2, MSH3, MUTYH, N4BP2, PMS1, PMS2, PMS2L3 (PMS2L9), TP73, TREX1
Other genes related to DNA repair	APEX2, ATM, ATRX, BTG2, CCNH, CDK7, CRY1, ERCC2 (XPD), GTF2H1, GTF2H2, IGHMBP2, LIG1, MNAT1, PCNA, RPA1, SUMO1
Mitochondria	
Membrane polarization & potential	BAK1, BCL2, BCL2L1, BNIP3, SOD1, TP53, UCP1, UCP2, UCP3
Mitochondrial transport	AIP, BAK1, BCL2, BCL2L1, BNIP3, CPT1B, CPT2, DNAJC19, FXC1 (TIMM10B), GRPEL1, HSP90AA1, HSPD1, IMMP2L, MFN2, MIPEP, MTX2, STARD3, TP53, TSPO, UCP1, UCP2, UCP3
Small molecule transport	SLC25A1, SLC25A10, SLC25A12, SLC25A13, SLC25A14, SLC25A15, SLC25A16, SLC25A17, SLC25A19, SLC25A2, SLC25A20, SLC25A21, SLC25A22, SLC25A23, SLC25A24, SLC25A25, SLC25A27, SLC25A3, SLC25A30, SLC25A31, SLC25A37, SLC25A4, SLC25A5
Targeting proteins to mitochondria	AIP, DNAJC19, FXC1 (TIMM10B), GRPEL1, HSPD1, IMMP2L, MFN2, MIPEP, TSPO
Mitochondrion protein import	AIP, COX10, COX18, DNAJC19, FXC1 (TIMM10B), GRPEL1, HSPD1, MIPEP, SH3GLB1
Outer membrane translocation	TOMM20, TOMM22, TOMM34, TOMM40, TOMM40L, TOMM70A
Inner membrane translocation	FXC1 (TIMM10B), IMMP1L, IMMP2L, OPA1, TAZ, TIMM10, TIMM17A, TIMM17B, TIMM22, TIMM23, TIMM44, TIMM50, TIMM8A, TIMM8B, TIMM9
Mitochondrial fission & fusion	COX10, COX18, FIS1, MFN1, MFN2, OPA1
Mitochondrial localization	DNM1L, LRPPRC, MFN2, MSTO1, NEFL, OPA1, RHOT1, RHOT2, UXT
Apoptotic genes	AIFM2, BAK1, BBC3, BCL2, BCL2L1, BID, BNIP3, CDKN2A, DNM1L, PMAIP1, SFN, SH3GLB1, SOD2, TP53
Hypoxia signaling	
Response to Hypoxia	ANGPTL4, ARNT2, CREBBP, EP300, HIF1A, MT3, PRKAA1
Response to oxidative stress	CAT, CYGB, GPX1, PIP3-E
Immune response	GPI, IL1A, IL6, IL6ST, NOS2A, NOTCH1, PTX3, RARA
Other genes related to stress response	ADM, EPO, HYOU1, VEGFA
Hemoglobin complex associated genes	CYGB, EPO, HBB, HMOX1, NOS2A, PIP3-E
Peroxidase	CAT, CYGB, GPX1, PIP3-E
Other oxidoreductase-related genes	HIF1AN, HMOX1, MT3, NOS2A, PLOD3, TH
Transcription co-factors	CREBBP, DR1, ENO1, EP300, EPAS1, HTATIP, RARA
Transcription factors	ARNT2, BHLHB2, CREBBP, ENO1, EP300, EPAS1, HIF1A, HIF3A, KHSRP, MYBL2, PPARA, RARA
Other transcription factors & regulators	HIF1AN, NOTCH1
Anti-apoptosis	BAX, ANGPTL4, BIRC5, IL1A, MYBL2, PEA15, PRKAA1, VEGFA
Caspase activity	BIRC5, CASP1

Induction of apoptosis	BAX, DAPK3, NUDT2
Other apoptosis genes	EP300
Signal transduction	ADM, ARNT2, CASP1, CDC42, CREBBP, EP300, EPAS1, EPO, GNA11, HIF1A, HIF3A, HMOX1, IGFBP1, IL1A, IL6, IL6ST, IQGAP1, KIT, LEP, PLAU, RARA, VEGFA
Protein biosynthesis	EEF1A1, PDIA2 (PDIP), PRKAA1, RPL28, RPL32, RPS2, RPS7
Protein heterodimerization	ARNT2, HIF1A, RARA, SAE1
Protein homodimerization	ARNT2, RARA, VEGFA
Protein amino acid phosphorylation	DAPK3, KIT, PRKAA1
Protein Binding	CASP1, CREBBP, ENO1, EP300, IQGAP1, NOS2A, PEA15, PPP2CB, RARA
Other genes related to protein metabolism	ARD1A, CDC42, GNA11, HYOU1, MAN2B1, PLOD3, PSMB3, SUMO2, TUBA4A (TUBA1)
Protease inhibitors	BIRC5, CSTB
Protease molecules	AGTPBP1, CASP1, ECE1, PLAU, PSMB3
Other extracellular molecules	ADM, ANGPTL4, CHGA, COL1A1, EPO, IGF2, IGFBP1, IL1A, IL6, LEP, NPY, PTX3, VEGFA
Cytoskeleton	DCTN2, SPTBN1
Cell cycle	BAX, BIRC5, EP300, HK2, IGF2, IL1A, MYBL2, SSSCA1, VEGFA
Cell proliferation	DCTN2, IGF2, IL1A, IL6, MT3, NPY, RARA, VEGFA
Growth factors	GPI, IGF2, IGFBP1, IL1A, IL6, KIT, VEGFA
Other genes related to cell growth	ENO1
Carbohydrate metabolism	GPI, HK2, LCT, MAN2B1, PEA15, PRKAA1, SLC2A1, SLC2A4
Lipid metabolism	AGPAT2, ANGPTL4, PPARA, PRKAA1
One-carbon compound metabolism	CA1
Superoxide metabolism	MT3, NOS2A
RNA metabolism	PRPF40A (FNBP3), KHSRP, RARA, RPL28, RPS2, SNRP70
Other genes related to metabolism	ADM, AGPAT2, MOCS3, NUDT2, TH, TST, UCP2
Cardiac excitation-contraction (E-C) coupling	ARNT2, CHGA, DAPK3, GNA11, IQGAP1, KIT, NOS2A, NOTCH1, NPY, PRKAA1, SPTBN1
TGF-β-BMP signaling PCR array	
TGF-β	TGFB1, TGFB2, TGFB3
BMP	BMP1, BMP2, BMP3, BMP4, BMP5, BMP6, BMP7
GDF	AMH, GDF2 (BMP9), GDF3 (Vgr-2), GDF5 (CDMP-1), GDF6, GDF7, IGF1, IGFBP3, IL6, INHA (inhibin a), INHBA (inhibin BA), LEFTY1, LTBP1, LTBP2, LTBP4, NODAL, PDGFB
Activin	INHA (inhibin a), INHBA (inhibin BA), INHBB (inhibin BB), LEFTY1, NODAL
Receptors	ACVR1 (ALK2), ACVR2A, ACVRL1 (ALK1), AMHR2, BMPR1A (ALK3), BMPR1B (ALK6), BMPR2, ITGB5 (integrin B5), ITGB7 (integrin B7), LTBP1, NR0B1, STAT1, TGFB1I1, TGFBR1, (ALK5) TGFBR2, TGFBR3, TGFBRAP1
SMAD	SMAD1 (MADH1), SMAD2 (MADH2), SMAD3 (MADH3), SMAD4 (MADH4), SMAD5 (MADH5)
TGF-β/activin-responsive	CDC25A, CDKN1A (p21WAF1 / p21CIP1), CDKN2B (p15LNK2B), COL1A1, COL1A2, COL3A1, FOS, GSC (goosecoid), IGF1, IGFBP3, IL6, ITGB5 (integrin B5), ITGB7 (integrin B7), JUN, JUNB, MYC, PDGFB, SERPINE 1 (PAI-1), TGFB1I1, TSC22D1 (TGFB1I4), TGFBI, TGIF1
BMP-responsive	BGLAP (osteocalcin), DLX2, ID1, ID2, JUNB, SOX4, STAT1
Molecules regulating signaling of the TGF-β superfamily	BAMBI, BMPER, CDKN2B (p15LNK2B), CER1 (cerberus), CHRD (chordin), CST3, ENG (Evi-1), EVI1, FKBP1B, FST (follistatin), HIPK2, NBL1 (DAN), NOG, PLAU (uPA), RUNX1 (AML1), SMURF1
Adhesion molecules	BGLAP (osteocalcin), ENG (Evi-1), ITGB5 (integrin B5), ITGB7 (integrin B7), TGFB1I1, TGFBI
Extracellular matrix structural constituents	BGLAP (osteocalcin), COL1A1, COL1A2, COL3A1, LTBP1, LTBP2, LTBP4, TGFBI
Other extracellular molecules	AMH, BMP1, BMP2, FST (follistatin), GDF2 (BMP9), GDF3 (Vgr-2), IGF1, IGFBP3, IL6, INHA (inhibin a), INHBA (inhibin BA), INHBB (inhibin BB), PDGFB, PLAU (uPA), SERPINE1
Transcription factors & regulators	DLX2, EVI1, FOS, GSC (goosecoid), HIPK2, ID1, JUN, JUNB, MYC, NR0B1, RUNX1 (AML1), SMAD1 (MADH1), SMAD2 (MADH2), SMAD3 (MADH3), SMAD4 (MADH4), SMAD5 (MADH5), SOX4, STAT1, TGFB1I1, TSC22D1 (TGFB1I4), TGIF1
Tumor necrosis factor (TNF) ligand and receptor	
Induction of apoptosis	FASLG, LTA, TNFSF10, TNFSF14, TNFSF8
Caspase activation	TNFSF15
Caspase inhibition	TNFSF14
Anti-apoptosis genes	CD40LG, TNF, TNFSF18
Other apoptosis-related genes	CD70 (TNFSF7), TNFSF9
Inflammatory response	CD40LG, TNF
NF-kB signaling pathway	FASLG, TNF, TNFSF10, TNFSF14, TNFSF15
Other TNF superfamily members	LTB, PGLYRP1, TNFSF11, TNFSF12, TNFSF13, TNFSF13B, TNFSF4, TNFSF5IP1
Induction of apoptosis	FAS, TNFRSF10A, TNFRSF10A, TNFRSF10B, TNFRSF19, TNFRSF25, CD27 (TNFRSF7), TNFRSF9, TRADD
Caspase activation	TNFRSF10A, TNFRSF10B

Caspase inhibition	CD27 (TNFRSF7)
Anti-apoptosis genes	FAS, TNFRSF10D, TNFRSF18, TNFRSF6B, CD27 (TNFRSF7)
Other apoptosis genes	CD40, LTBR, NGFR, TNFRSF10C, TNFRSF11B, TNFRSF12A, TNFRSF14, TNFRSF1A, TNFRSF1B, TNFRSF21
Inflammatory response	CD40, TNFRSF1A
NF-kB signaling pathway	CD40, EDA2R, LTBR, TNFRSF10A, TNFRSF10B, TNFRSF1A, CD27 (TNFRSF7), TRADD
JNK signaling pathway	EDA2R, TNFRSF19, CD27 (TNFRSF7)
Other TNF receptor superfamily members	TNFRSF11A, TNFRSF13B, TNFRSF13C, TNFRSF17, TNFRSF19L, TNFRSF4, TNFRSF8
Induction of apoptosis	CASP3, CRADD, FADD, TRADD
Caspases	CASP2, CASP3, CASP8
Anti-apoptosis genes	BAG4, CASP2, TNF
Other apoptosis genes	DFFA, PAK1, TNFRSF1A, TRAF2
Inflammatory response	TNF, TNFRSF1A
NF-kB signaling pathway	CASP8, FADD, TNF, TNFRSF1A, TRADD
JNK signaling pathway	MAP2K4, MAPK8, PAK1
Transcription regulators	JUN, PARP1, RB1, TNF, TNFRSF1A
TNFR1 signaling pathway	ARHGDIB, CAD, HRB, LMNA, LMNB1, LMNB2, MADD, MAP3K1, MAP3K7, PAK2, PRKDC, SPTAN1
Induction of apoptosis	IKBKG, LTA, TRAF3
Anti-apoptosis genes	NFKB1, TNFAIP3
Other apoptosis genes	NFKBIA, TNFRSF1B, TRAF1, TRAF2
Inflammatory response	NFKB1
NF-kB signaling pathway	CHUK, IKBKB, IKBKG, NFKBIA, TNFAIP3
Transcription regulators	IKBKB, IKBKG, NFKB1, NFKBIA
TNFR2 signaling pathway	DUSP1, HRB, IKBKAP, MAP3K1, MAP3K14, TANK

Supplement T2 – Lists of oxidative-response genes in the pathways shown in Supplement T1

Unigene	Symbol	Description
Hs.470316	ACVR1	Activin A receptor, type I
Hs.470174	ACVR2A	Activin A receptor, type IIA
Hs.591026	ACVRL1	Activin A receptor type II-like 1
Hs.112432	AMH	Anti-Mullerian hormone
Hs.659889	AMHR2	Anti-Mullerian hormone receptor, type II
Hs.533336	BAMBI	BMP and activin membrane-bound inhibitor homolog (*Xenopus laevis*)
Hs.654541	BGLAP	Bone gamma-carboxyglutamate (gla) protein
Hs.1274	BMP1	Bone morphogenetic protein 1
Hs.73853	BMP2	Bone morphogenetic protein 2
Hs.387411	BMP3	Bone morphogenetic protein 3
Hs.68879	BMP4	Bone morphogenetic protein 4
Hs.296648	BMP5	Bone morphogenetic protein 5
Hs.285671	BMP6	Bone morphogenetic protein 6
Hs.473163	BMP7	Bone morphogenetic protein 7
Hs.660998	BMPER	BMP binding endothelial regulator
Hs.524477	BMPR1A	Bone morphogenetic protein receptor, type IA
Hs.598475	BMPR1B	Bone morphogenetic protein receptor, type IB
Hs.471119	BMPR2	Bone morphogenetic protein receptor, type II (serine/threonine kinase)
Hs.437705	CDC25A	Cell division cycle 25 homolog A (*S. pombe*)
Hs.370771	CDKN1A	Cyclin-dependent kinase inhibitor 1A (p21, Cip1)
Hs.72901	CDKN2B	Cyclin-dependent kinase inhibitor 2B (p15, inhibits CDK4)
Hs.248204	CER1	Cerberus 1, cysteine knot superfamily, homolog (*Xenopus laevis*)
Hs.166186	CHRD	Chordin
Hs.172928	COL1A1	Collagen, type I, alpha 1
Hs.489142	COL1A2	Collagen, type I, alpha 2
Hs.443625	COL3A1	Collagen, type III, alpha 1
Hs.304682	CST3	Cystatin C
Hs.419	DLX2	Distal-less homeobox 2
Hs.76753	ENG	Endoglin
Hs.656395	EVI1	Ecotropic viral integration site 1
Hs.709461	FKBP1B	FK506 binding protein 1B, 12.6 kDa
Hs.25647	FOS	V-fos FBJ murine osteosarcoma viral oncogene homolog
Hs.9914	FST	Follistatin
Hs.279463	GDF2	Growth differentiation factor 2
Hs.86232	GDF3	Growth differentiation factor 3
Hs.1573	GDF5	Growth differentiation factor 5
Hs.492277	GDF6	Growth differentiation factor 6
Hs.447688	GDF7	Growth differentiation factor 7
Hs.440438	GSC	Goosecoid homeobox
Hs.632033	HIPK2	Homeodomain interacting protein kinase 2
Hs.504609	ID1	Inhibitor of DNA binding 1, dominant negative helix-loop-helix protein
Hs.180919	ID2	Inhibitor of DNA binding 2, dominant negative helix-loop-helix protein
Hs.160562	IGF1	Insulin-like growth factor 1 (somatomedin C)
Hs.450230	IGFBP3	Insulin-like growth factor binding protein 3
Hs.654458	IL6	Interleukin 6 (interferon, beta 2)

Hs.407506	INHA	Inhibin, alpha
Hs.583348	INHBA	Inhibin, beta A
Hs.1735	INHBB	Inhibin, beta B
Hs.536663	ITGB5	Integrin, beta 5
Hs.654470	ITGB7	Integrin, beta 7
Hs.714791	JUN	Jun oncogene
Hs.25292	JUNB	Jun B proto-oncogene
Hs.656214	LEFTY1	Left-right determination factor 1
Hs.713533	LTBP1	Latent transforming growth factor beta binding protein 1
Hs.512776	LTBP2	Latent transforming growth factor beta binding protein 2
Hs.466766	LTBP4	Latent transforming growth factor beta binding protein 4
Hs.202453	MYC	V-myc myelocytomatosis viral oncogene homolog (avian)
Hs.654502	NBL1	Neuroblastoma, suppression of tumorigenicity 1
Hs.370414	NODAL	Nodal homolog (mouse)
Hs.248201	NOG	Noggin
Hs.268490	NR0B1	Nuclear receptor subfamily 0, group B, member 1
Hs.1976	PDGFB	Platelet-derived growth factor beta polypeptide (simian sarcoma viral (v-sis) oncogene homolog)
Hs.77274	PLAU	Plasminogen activator, urokinase
Hs.149261	RUNX1	Runt-related transcription factor 1
Hs.414795	SERPINE1	Serpin peptidase inhibitor, clade E (nexin, plasminogen activator inhibitor type 1), member 1
Hs.604588	SMAD1	SMAD family member 1
Hs.12253	SMAD2	SMAD family member 2
Hs.714621	SMAD3	SMAD family member 3
Hs.75862	SMAD4	SMAD family member 4
Hs.167700	SMAD5	SMAD family member 5
Hs.189329	SMURF1	SMAD specific E3 ubiquitin protein ligase 1
Hs.643910	SOX4	SRY (sex determining region Y)-box 4
Hs.642990	STAT1	Signal transducer and activator of transcription 1, 91kDa
Hs.645227	TGFB1	Transforming growth factor, beta 1
Hs.513530	TGFB1I1	Transforming growth factor beta 1 induced transcript 1
Hs.507916	TSC22D1	TSC22 domain family, member 1
Hs.133379	TGFB2	Transforming growth factor, beta 2
Hs.592317	TGFB3	Transforming growth factor, beta 3
Hs.369397	TGFBI	Transforming growth factor, beta-induced, 68kDa
Hs.494622	TGFBR1	Transforming growth factor, beta receptor 1
Hs.604277	TGFBR2	Transforming growth factor, beta receptor II (70/80kDa)
Hs.482390	TGFBR3	Transforming growth factor, beta receptor III
Hs.446350	TGFBRAP1	Transforming growth factor, beta receptor associated protein 1
Hs.373550	TGIF1	TGFB-induced factor homeobox 1
Hs.534255	B2M	Beta-2-microglobulin
Hs.412707	HPRT1	Hypoxanthine phosphoribosyltransferase 1
Hs.523185	RPL13A	Ribosomal protein L13a
Hs.592355	GAPDH	Glyceraldehyde-3-phosphate dehydrogenase
Hs.520640	ACTB	Actin, beta
N/A	HGDC	Human Genomic DNA Contamination
Hs.431048	ABL1	C-abl oncogene 1, receptor tyrosine kinase
Hs.601206	ANKRD17	Ankyrin repeat domain 17
Hs.73722	APEX1	APEX nuclease (multifunctional DNA repair enzyme) 1
Hs.367437	ATM	Ataxia telangiectasia mutated
Hs.271791	ATR	Ataxia telangiectasia and Rad3 related
Hs.533526	ATRX	Alpha thalassemia/mental retardation syndrome X-linked (RAD54 homolog, *S. cerevisiae*)
Hs.194143	BRCA1	Breast cancer 1, early onset
Hs.519162	BTG2	BTG family, member 2
Hs.292524	CCNH	Cyclin H
Hs.184298	CDK7	Cyclin-dependent kinase 7
Hs.24529	CHEK1	CHK1 checkpoint homolog (*S. pombe*)
Hs.291363	CHEK2	CHK2 checkpoint homolog (*S. pombe*)
Hs.135471	CIB1	Calcium and integrin binding 1 (calmyrin)
Hs.249129	CIDEA	Cell death-inducing DFFA-like effector a
Hs.151573	CRY1	Cryptochrome 1 (photolyase-like)
Hs.290758	DDB1	Damage-specific DNA binding protein 1, 127kDa
Hs.505777	DDIT3	DNA-damage-inducible transcript 3
Hs.339396	DMC1	DMC1 dosage suppressor of mck1 homolog, meiosis-specific homologous recombination (yeast)
Hs.435981	ERCC1	Excision repair cross-complementing rodent repair deficiency, complementation group 1 (includes overlapping antisense sequence)
Hs.487294	ERCC2	Excision repair cross-complementing rodent repair deficiency, complementation group 2
Hs.498248	EXO1	Exonuclease 1
Hs.591084	FANCG	Fanconi anemia, complementation group G
Hs.409065	FEN1	Flap structure-specific endonuclease 1
Hs.292493	XRCC6	X-ray repair complementing defective repair in Chinese hamster cells 6
Hs.80409	GADD45A	Growth arrest and DNA-damage-inducible, alpha
Hs.9701	GADD45G	Growth arrest and DNA-damage-inducible, gamma
Hs.661218	GML	Glycosylphosphatidylinositol anchored molecule like protein
Hs.577202	GTF2H1	General transcription factor IIH, polypeptide 1, 62kDa
Hs.191356	GTF2H2	General transcription factor IIH, polypeptide 2, 44kDa
Hs.386189	GTSE1	G-2 and S-phase expressed 1
Hs.152983	HUS1	HUS1 checkpoint homolog (*S. pombe*)
Hs.503048	IGHMBP2	Immunoglobulin mu binding protein 2
Hs.17253	IP6K3	Inositol hexakisphosphate kinase 3
Hs.61188	XRCC6BP1	XRCC6 binding protein 1
Hs.1770	LIG1	Ligase I, DNA, ATP-dependent
Hs.463978	MAP2K6	Mitogen-activated protein kinase kinase 6
Hs.432642	MAPK12	Mitogen-activated protein kinase 12
Hs.35947	MBD4	Methyl-CpG binding domain protein 4
Hs.195364	MLH1	MutL homolog 1, colon cancer, non-polyposis type 2 (E. coli)
Hs.436650	MLH3	MutL homolog 3 (*E. coli*)
Hs.509523	MNAT1	Menage-a-trois homolog 1, cyclin H assembly factor (*Xenopus laevis*)

Hs.459596	MPG	N-methylpurine-DNA glycosylase
Hs.192649	MRE11A	MRE11 meiotic recombination 11 homolog A (*S. cerevisiae*)
Hs.597656	MSH2	MutS homolog 2, colon cancer, non-polyposis type 1 (E. coli)
Hs.280987	MSH3	MutS homolog 3 (*E. coli*)
Hs.271353	MUTYH	MutY homolog (*E. coli*)
Hs.391463	N4BP2	Nedd4 binding protein 2
Hs.492208	NBN	Nibrin
Hs.66196	NTHL1	Nth endonuclease III-like 1 (*E. coli*)
Hs.380271	OGG1	8-Oxoguanine DNA glycosylase
Hs.20930	PCBP4	Poly(rC) binding protein 4
Hs.147433	PCNA	Proliferating cell nuclear antigen
Hs.424932	AIFM1	Apoptosis-inducing factor, mitochondrion-associated, 1
Hs.111749	PMS1	PMS1 postmeiotic segregation increased 1 (*S. cerevisiae*)
Hs.632637	PMS2	PMS2 postmeiotic segregation increased 2 (*S. cerevisiae*)
Hs.225784	PMS2L3	Postmeiotic segregation increased 2-like 3
Hs.78016	PNKP	Polynucleotide kinase 3'-phosphatase
Hs.631593	PPP1R15A	Protein phosphatase 1, regulatory (inhibitor) subunit 15A
Hs.491682	PRKDC	Protein kinase, DNA-activated, catalytic polypeptide
Hs.531879	RAD1	RAD1 homolog (*S. pombe*)
Hs.16184	RAD17	RAD17 homolog (*S. pombe*)
Hs.375684	RAD18	RAD18 homolog (*S. cerevisiae*)
Hs.81848	RAD21	RAD21 homolog (*S. pombe*)
Hs.655835	RAD50	RAD50 homolog (*S. cerevisiae*)
Hs.631709	RAD51	RAD51 homolog (RecA homolog, *E. coli*) (*S. cerevisiae*)
Hs.172587	RAD51L1	RAD51-like 1 (*S. cerevisiae*)
Hs.655354	RAD9A	RAD9 homolog A (*S. pombe*)
Hs.546282	RBBP8	Retinoblastoma binding protein 8
Hs.443077	REV1	REV1 homolog (*S. cerevisiae*)
Hs.461925	RPA1	Replication protein A1, 70 kDa
Hs.408846	SEMA4A	Sema domain, immunoglobulin domain (Ig), transmembrane domain (TM) and short cytoplasmic domain, (semaphorin) 4A
Hs.591336	SESN1	Sestrin 1
Hs.211602	SMC1A	Structural maintenance of chromosomes 1A
Hs.81424	SUMO1	SMT3 suppressor of mif two 3 homolog 1 (*S. cerevisiae*)
Hs.654481	TP53	Tumor protein p53
Hs.697294	TP73	Tumor protein p73
Hs.707026	TREX1	Three prime repair exonuclease 1
Hs.191334	UNG	Uracil-DNA glycosylase
Hs.654364	XPA	*Xeroderma pigmentosum*, complementation group A
Hs.475538	XPC	*Xeroderma pigmentosum*, complementation group C
Hs.98493	XRCC1	X-ray repair complementing defective repair in Chinese hamster cells 1
Hs.647093	XRCC2	X-ray repair complementing defective repair in Chinese hamster cells 2
Hs.592325	XRCC3	X-ray repair complementing defective repair in Chinese hamster cells 3
Hs.444451	ZAK	Sterile alpha motif and leucine zipper containing kinase AZK

Importance of CDK7 for G1 Re-Entry into the Mammalian Cell Cycle and Identification of New Downstream Networks Using a Computational Method

Hideko Sone[*,1,2,§], Tomokazu Fukuda[3,§], Hiroyoshi Toyoshiba[1,§], Takeharu Yamanaka[1], Fred Parham[1] and Christopher J. Portier[1]

[1]*Laboratory of Computational Biology and Risk Analysis, National Institute of Environmental Health Sciences, 111 T.W. Alexander Drive, Research Triangle Park, NC 27709, USA*

[2]*Health Effects Team, National Institute for Environmental Studies, 16-2 Onogawa, Tsukuba 305-8506, Japan*

[3]*Laboratory of Animal breeding and Genetics, Graduate school of Agricultural Science, Tohoku University, Tsutsumidori-amamiyamachi 1-1 Aoba-ku, Sendai 981-8555, Japan*

Abstract: Many of the key molecules in cell cycle progression (e.g. pRB, cyclin complexes) and their basic interactions are oncogene or tumor suppressor genes, which are well characterized in the clinical and experimental analysis. However, there are still unknown mechanisms for the cell cycle regulation, which is critical step for the progression of the cancer development. Especially it is not fully understood how the cells move to G1 phase from quiescent G0 phase in the mammalian cells. To find out the new gene networks associated with the two transition of the mammalian cell cycle (G0 to G1 and G1 to S phase), we analyzed the linkages between 39 representative oncogene or tumor suppressor genes, which related to the cell cycle regulation, with gene expression sets obtained from the publicly opened microarray data for mouse embryonic fibroblasts that synchronized by the serum starvation or hydroxyurea treatment. Analyses with a qualitative algorithm based on Bayesian networks that assume a log-linear relationship between genes have applied, and newly found networks were validated. Results highlighted the importance of two master genes, *Cdk7* and *Cdkna2* for the re-entry to G1 from G0, and suggested a new network connection from *Cdk7* to downstream molecules, including the *EGF* receptor and *N-myc*. Introduction of a recombinant *Cdk7* with retrovirus decreased endogenous EGFR and N-myc protein levels. The results supported the computational prediction of the *Cdk7* network. Taken together, these result showed the existence of new regulating pathway from Cdk7 to Egfr and N-myc, suggesting this analytical approach provides an assessment of regulatory networks in complex mammalian cells, and the process of the carcinogenesis.

Keywords: Gene network, cell cycle, Cdk7, mammalian, Bayesian theory.

INTRODUCTION

Cell division and tissue growth represent two of the most fundamental biological processes and play essential roles in development, aging, cancer [1, 2], and many other diverse events. Although gene transcripts have been comprehensively catalogued in yeast, much work remains to be done in higher organisms. Especially, for tumor progression, the gene networks underlying the regulation of the cell cycle are not well understood in cancer cells or the initiated precancerous cells. Several groups have utilized microarrays to perform serial analyses of gene expression during cellular replication in normal or cancer human and mouse cell lines [3-6]. These microarray data have been analyzed using clustering approaches such as hierarchical clustering and k-means to identify stage-specific or co-regulated genes through each phase of the cell cycle. However, these methodologies can only identify genes with expression levels that correlate over time, and the network dynamics of the cell cycle is not yet fully understood.

Integrated and networked functions in mammalian cells can be identified and quantified through the use of a computational model. Efforts to systematically define specific gene network structures to further understand the functions and dynamics of each gene and its protein products have lead to a new generation of *in silico* analysis tools that use diagrams to depict the logical relationships between genes [7-9]. To infer unknown gene networks from microarray gene expression data, the methods adopted need to incorporate the two different aspects of Bayesian models and associated validation tools. The application of these biostatistical methods has the potential to elucidate unknown mechanisms underlying the key regulatory systems of mammalian cells [10-12].

The regulatory mechanisms for the G0 quiescent stage of the cell cycle remain largely unknown. For the efficient progression from the G0 to G1 phase, the protein level of the p27/kip1 is known to have a important role in T cell from *in vitro* study and a knockout mouse study [13, 14]. In the normal cells, the protein level of p27 is high during G0 phase

*Address correspondence to this author at the Research Center for Environmental Risk, National Institute for Environmental Studies, 16-2 Onogawa, Tsukuba 305-8506, Japan; Tel: +81.298.50.2464; Fax: +81.298.50.2546; E-mail: hsone@nies.go.jp

§These authors equally contributed to this work.

1876-3901/10

but decreases rapidly on the entry to G1 [14, 15]. The degradation of p27 is controlled by an SCF complex, which involves SKP2 [16, 17]. Although these findings for G0-G1 regulation have had a significant impact, it is not clear whether these mechanisms can be applied to the all type of cells and tissues. For cancer therapeutics, the G0-G1 transition of the cell cycle has been a strong target to prevent tumor growth and progression [18-20].

In our current study, we employed the gene datasets from the publicly opened microarray data for the mouse fibroblasts, which synchronized with the serum starvation and hydroxyarea, which are the study of the transition from a quiescent state into the cell cycle in mouse embryonic fibroblast (MEF) cells reported by Ishida *et al.* [4]. In order to elucidate new gene networks related to the progression of the cell cycle, the gene expression datasets were analyzed using a series of approaches in which putative network structures are elucidated using Bayesian networks. These approaches involve a likelihood-based selection algorithm to qualitatively infer the identity of the network structure [21] and a quantitative algorithm involving a Markov chain Monte Carlo (MCMC) method [22, 23] is then used to quantify the structure. The identified interactions between genes that are based upon these predicted gene networks were then validated using a retrovirus expression system.

MATERIALS AND METHODS

Microarray Data Sets

Previously published mouse embryonic fibroblast (MEF) cell microarray datasets were used in our analyses [4]. Briefly, the cells were synchronized by either serum starvation or hydroxyurea treatment. We used the data sets obtained from the serum starved cells for the analysis of re-entry into G1 from G0 (0, 6, 12, 15, 18, 21, 24 hours after serum starvation), and those from the hydroxyurea exposed fibroblasts for the G1-S analysis (0, 3, 6, 9, 12, 15, 18 hours after the treatment). The detailed methods used to obtain these microarray data have been previously described [4].

Selection of the Subset Database

The original gene expression data, comprising about 6437 genes, were screened for genes that showed at least a 2.0-fold change (up- or down-regulation) using GenMAPP [24]. The distribution and frequency of the fold changes (relative to the time 0) at each time point were analyzed by MAPFinder 1.0 beta, an accessory tool of GenMAPP, to identify the optimal biological maps. From this collection of maps, we selected those related to cell cycle processes that had a "z" score greater than 1.95 (the z score represents the difference between the observed number of genes meeting the criteria and the expected number of genes meeting the criteria in each map based on gene ontology). As detailed in Table **1**, 10 maps were selected based on gene ontology (denoted MAPP) and the relationship to the cell cycle. A subset of 39 genes was chosen from among the MAPP maps selected (Table **2**). The abbreviated names of the genes that were analyzed in this report are presented according to the displays listed in GenMAPP.

Mathematical Models

We applied the expression-associated network modeling method previously developed by Yamanaka *et al.* [21] to the

Table 1. List of Maps with More than 1.95 Z Score Selected from Maps Analyzed by MAPFinder. Maps are the Database from Mouse Biological Processes that are Contain in GenMAPP

MAPP Name	A	B	C	D	E	R	z Score	Time Point
Mm_cell cycle	4	15	104	26.7	14.4	95	2.014	18h
	4	15	104	26.7	14.4	87	2.211	21h
Mm_cell cycle arrest	2	2	11	100	18.2	92	4.175	12h
	2	2	11	100	18.2	92	4.175	15h
	2	2	11	100	18.2	109	3.795	18h
	2	2	11	100	18.2	118	3.626	21h
	2	2	11	100	18.2	121	4.335	24h
Mm_cell cycle control	15	48	124	31.2	38.7	132	3.205	12h
	9	48	124	18.8	38.7	87	2.102	21h
Mm_cell growth and or maintenance	17	55	153	30.9	35.9	132	3.357	12h
Mm_cell growth	3	7	16	42.9	43.8	118	2.317	21h
Mm_cell proliferation	3	4	28	75	14.3	95	4.177	18h
Mm_G1 S transition of	1	1	5	100	20	101	2.771	6h
Mitotic cell cycle								
Mm_mitosis	2	6	23	33.3	26.1	87	1.95	21h
Mm_mitotic cell cycle	1	1	7	100	14.3	101	2.771	6h
Mm_M phase of mitotic cell cycle	2	6	23	33.3	26.1	87	1.95	21h

A, the number of genes meeting the criterion in this specific MAPP; B, the total number of genes measured in this specific MAPP; C, Number on MAPP; D, Percent Changed; E, Percent present; N, the total number of genes measured (= 894), R, the total number of distinct genes meeting the criterion. Criterions were set at > 2.0 or < 0.5 of the expression ratio. Each time point means a sampling time after serum starvation. Z Score= (A-B*R/N)/√(B(R/N)(1-R/N)(1-B-1/N-1)).

Table 2. List of Name Abbreviations and Description of the Genes Analyzed in this Study

Gene Name	Description
Abl1	Mouse c-abl gene exon 1 of type II
Ccna1	Mouse mRNA for cyclin A1
Ccna2	Mouse mRNA for cyclin A2
Ccnb2	Mouse mRNA for cyclin B2
Ccne1	Mouse mRNA for cyclin E
Crkol	Mouse mRNA for Crkl protein
Csf1r	Mouse c-fms proto-oncogene
E2f5	Mouse mRNA for E2F-5 protein
Egfr	Mouse (BALB/c) Epidermal Growth Factor Receptor mRNA
Elk1	Mouse mRNA for elk1 protein
Elk4	Mouse sap1A mRNA
Ets1	Mouse ets-1 mRNA
Etv6	Mouse mRNA for TEL protein
Fgf3	Mouse int-2 gene
Figf	Mouse mRNA for new member of PDGF/VEGT family of growth factors
Fos	Mouse c-fos oncogene
Fosb	Mouse fosB mRNA
Il1a	Mouse mRNA for interleukin-1
Lmyc1	Mouse L-myc gene
Mybl2	Mouse B-myb mRNA
Myc	Mouse normal c-myc gene
Nmyc1	Mouse N-myc gene
Nras	Mouse mRNA for N-ras protein (exons 1 - 6 part.)
Pdgfb	Mouse platelet-derived growth factor B chain (c-sis) gene
Pgf	Mouse mRNA for placenta growth factor
Ptn	Mouse mRNA for OSF-1
Ret	Mouse mRNA for ret proto-oncogene
Tfdp1	Mouse mRNA for DRTF-polypeptide-1 (DP-1)
Tgfb2	Mouse mRNA for transforming growth factor-beta2
Thra	Mouse c-erbA-alpha mRNA for thyroid hormone receptor
Tlm	Mouse tlm oncogene for tlm protein
Cdkn2a	Mouse CDK4 and CDK6 inhibitor protein (p16ink4a)
Cdkn2d	Mouse p19 protein mRNA, complete cds
E2F1	Mouse E2F1 mRNA, complete cds
p53	Mouse mRNA for cellular tumour antigen p53
mdm2	Mouse mdm2 mRNA for mdm2 protein
Cdk7	Mouse mRNA for protein kinase crk4
Rbl1	Mouse p107 (p107) mRNA, complete cds
Rbl2	Mouse retinoblastoma-related protein Rb2/p130

fold-change data from the gene-expression data sets. This method falls under the general area of Bayesian networks, with a likelihood-based selection algorithm used to identify the most promising networks. In general, if $\boldsymbol{X_1}$, $\boldsymbol{X_2}$....$\boldsymbol{X_p}$ represents the data obtained for p genes, N denotes a network, and θ denotes parameters in that network, with the likelihood given by:

$$f_{X|N,\theta}(X_1, X_2, ..., X_p \mid N, \theta) = \prod_{j=1}^{p} f_{X_j|N,\theta_j}(X_j \mid pa(X_j), N, \theta_j) \quad (1)$$

A. The choice of the best network would be the one with the largest value of the posterior density at the chosen network topology; that is

$$\text{find } \hat{N} = \arg\max_{N} f_{N|D}(N \mid D) \quad (2)$$

$$\text{where } f_{N|D}(N \mid D) \propto f_N(N) \cdot f_{D|N}(D \mid N) \quad (3)$$

B. The Bayesian network used in this analysis had the following assumptions:

$$\text{i) } f_N(N) \Rightarrow \text{ uniform distribution} \quad (4)$$

$$\text{ii) } f_{D|\theta,N}(D \mid \theta, N) = \prod_{j=1}^{p} \left\{ \prod_{i=1}^{n} f_{X_j|N,\theta_j}(X_{ji} \mid pa(X_{ji}), N, \theta_j) \right\} \quad (5)$$

$$\text{iii) } f_{\theta|N}(\theta \mid N) = \prod_{j=1}^{p} f_{\theta_j|N}(\theta_j \mid N) \quad (6)$$

where pa (X_{ji}) is the collection of genes that link to the j^{th} gene in the network (a pathway).

with these assumptions,

$$\log f_{N|D}(N \mid D) \propto \sum_{j=1}^{p} \log \int \left\{ \prod_{i=1}^{n} f_{X_j|N,\theta_j}(X_{ji} \mid pa(X_{ji}), N, \theta_j) \right\} \cdot f(\theta_j \mid N) d\theta_j \quad (7)$$

Thus, it is possible to focus on each gene rather than the whole network and still obtain a global optimum. To quantify rates in the gene-expression network, we used the Bayesian methods developed by Toyoshiba *et al.* [22, 23]. Supposing that $\boldsymbol{X_i}$ (i=*1,2,3...p*) represents the natural log of the relative ratio, the functional relationships between the genes could be characterized using the log-linear model below:

$$E(X_i \mid Pa(X_i), \beta_{i\bullet}) = e^{\sum_{j=1}^{p} I_{ji}\beta_{ji}X_j} \quad (8)$$

where I_{ji} is an indicator function (-1, 0, 1) characterizing the effect from $\boldsymbol{G_j}$ to $\boldsymbol{G_i}$, T represents a matrix having I_{ij} as the (i,j) element, and $\beta_{i\bullet}=[\beta_{j1}, \beta_{j2}\beta_{j3}\beta_{j4}...\beta_{jp}]$ is the vector in which each β_{ji} is the magnitude by which one unit of gene $\boldsymbol{X_j}$ will affect the expression levels of gene $\boldsymbol{X_i}$. Thus, if *Iji* is not equal to 0, ***Pa(Xi)*** contains $\boldsymbol{X_j}$.

If $f(\boldsymbol{X_i} \mid T, \theta)$ is defined as the distribution of gene expression in the given model, then the likelihood is written as

$$f_{X|T,\theta}(X_1, X_2, ...X_P \mid T, \theta) = \prod_{j=1}^{p} f_{X_j|T,Pa(X_j),\theta}(X_j \mid T, Pa(X_j), \theta), \quad (9)$$

where θ represents the parameter vector in the model.

By Bayes' theorem, the prior distribution is given by

$$f_{\theta|X,T}(\theta \mid X,T) \sim f_{X|T,\theta}(X_1, X_2, ...X_P \mid T,\theta) \cdot f_\theta(\theta) \quad (10)$$

The posterior distributions $f_{\theta|X,T}$ were evaluated using the MCMC method. In our analyses, $f_{X|T,\theta}$ was assumed to be normal, with a mean defined by equation (8) and a random variance whose prior distribution was assumed to be uniform with 0 as the lower bound and twice the maximum STD for each gene distribution. The prior distribution for θ and f_θ was assumed to be lognormal with a mean of 0 and a variance of 1.0

The MCMC analysis was applied as described in [23] and [22]. A typical MCMC run was 100,000 samples with the first 20% of the samples discarded to "burn in" the algorithm. Some runs were much longer depending on convergence and stabilization of the resulting posterior distributions.

The model described in this section is an analysis tool and is not intended to characterize the mechanisms by which the different genes are linked. Instead, it is intended to find the most prominent linkages between cells to provide hypotheses that can be further explored and later modeled mechanistically.

Visualization of Gene Networks and Clustering Analysis

We used a MATLAB script newly developed by Parham *et al.* (unpublished data) to generate transcriptional regulatory networks using MATLAB version 6.5 (The MathWorks, Inc., Natick, MA).

Establishment of Mouse *CDK7* Recombinant Retrovirus

A full length cDNA fragment of mouse cyclin-dependent kinase (*Cdk*)*7* (NIH Mammalian Gene bank accession number: NMV009874) was obtained by RT-PCR from the total RNA extracts of 13.5 day mouse embryo using a previously described method [25]. A hemagglutinin (HA) protein tag sequence was then introduced at the carboxyl terminus of this mouse *Cdk7* cDNA using a tailed PCR method. The *Cdk7* cDNA was next subcloned into the EcoRV site of pBluescript SKII+ (Stratagene, La Jolla, CA) by blunt end ligation, and the resulting constructs were validated using a cycle sequencing reaction in an ABI 310 genetic analyzer (Applied Biosystems, Foster City, CA). The subcloned *Cdk7* cDNA fragment was then transferred into the multiple cloning site of an LXIN retrovirus vector (Clontech, Mountain View, CA). Both empty LXIN vector and LXIN vector harboring the mouse *Cdk7* cDNA were introduced into PT67 retrovirus packaging cells (Clontech) using Fugene6 (Roche, Basel, Switzerland). Infected cells were then selected with 1mg/ml G418 (Invitrogen, Carlsbad, CA) in the growth media for one week.

Measurement of the Retrovirus Titers in the Producer Cells

Conditioned medium from the producer cells was diluted 1:10 and 1:50 with DMEM containing 10% calf serum, and then used for the infection of NIH3T3 cells to measure the titer of the synthesized retrovirus. NIH3T3 cells were grown in media with diluted retroviruses for two days under the same conditions that are described below for mouse embryonic fibroblasts. The infected NIH3T3 cells were diluted 1:100 and 1:1000, and then selected with 1mg/ml G418 for one week. Retrovirus titers of the original conditioned medium were calculated based on the number of colonies demonstrating G418 resistance.

Preparation of MEF Cells that Expresses the Recombinant Mouse *CDK7*

Mouse embryonic fibroblasts (MEF) were prepared using a previously described method [25]. Second passage primary fibroblasts at a 70% confluency were infected with conditioned medium containing PT67 producer cells at a 1:2 dilution 1:2 with basal MEF medium for 2 days in the presence of 1μg/ml polybrene (Sigma-Aldrich, St. Louis, MO). When the infected MEF cells reached confluence, they were diluted 1:5 as above and selected with 200μg/ml G418 for one week. Control experiments confirmed that non-infected MEF cells did not survive in the presence of 200μg/ml G418 (data not shown). Infected cells selected with G418 were subjected to lysis and protein extraction for western blot analyses.

Western Blot Analyses of MEF Cells Exogenously Expressing Mouse *CDK7*

Total proteins were isolated from MEF cells infected with either control or Cdk7 recombinant retrovirus using a standard methodology [25]. Heat-denatured proteins were separated by 10% SDS-PAGE and the proteins in the gel were transferred to polyvinylidene difluoride (PVDF) membranes (Immobilon P, Millipore, Billerica, MA). After blocking with 1% non-fat dry milk-Tris buffered saline and 0.1% Tween 20 (TBST), the membranes were probed with anti-HA (High affinity HA 3F10, 1:5,000 dilution, Roche), anti-α-CDK7 (sc-723, 1:5,000 dilution, Santa Cruz, CA), anti-EGFR (kindly provided by Dr. DiAugustine, RP) and anti-N-MYC1 (sc-791, 1:1,000 dilution, Santa Cruz, CA) and anti-c-FOS (sc-52, 1:1,000 dilution, Santa Cruz, CA)antibodies. Blots were then incubated with horseradish peroxidase (HRP)-conjugated rabbit anti-rat IgG (A5795, 1:5,000 dilution, Roche) or donkey anti-rabbit IgG (1:5,000 dilution, GE Healthcare Bioscience) secondary antibodies, respectively. Immunoreactive proteins were detected by enhanced chemiluminescence (P90720, Millipore). Signal intensities from the western blots were detected with X-ray film and quantified using NIH3T3 image software.

RESULTS

Strategy and Analysis of Gene Network Structures

Our experimental strategy is illustrated in Fig. (**1**) and consists of three steps: selection of datasets, visualization and analysis by mathematical modeling, and prediction of biological function through the analysis of transcripts. Genome-wide expression data can provide information linking diverse genes and may be useful as a classification tool to identify alterations in biological processes linked to disease. In contrast, carefully designed analyses of a limited gene group associated with a specific biological process can be used to quantify the dynamics of a gene regulatory network. The genes associated with cell cycle regulation are

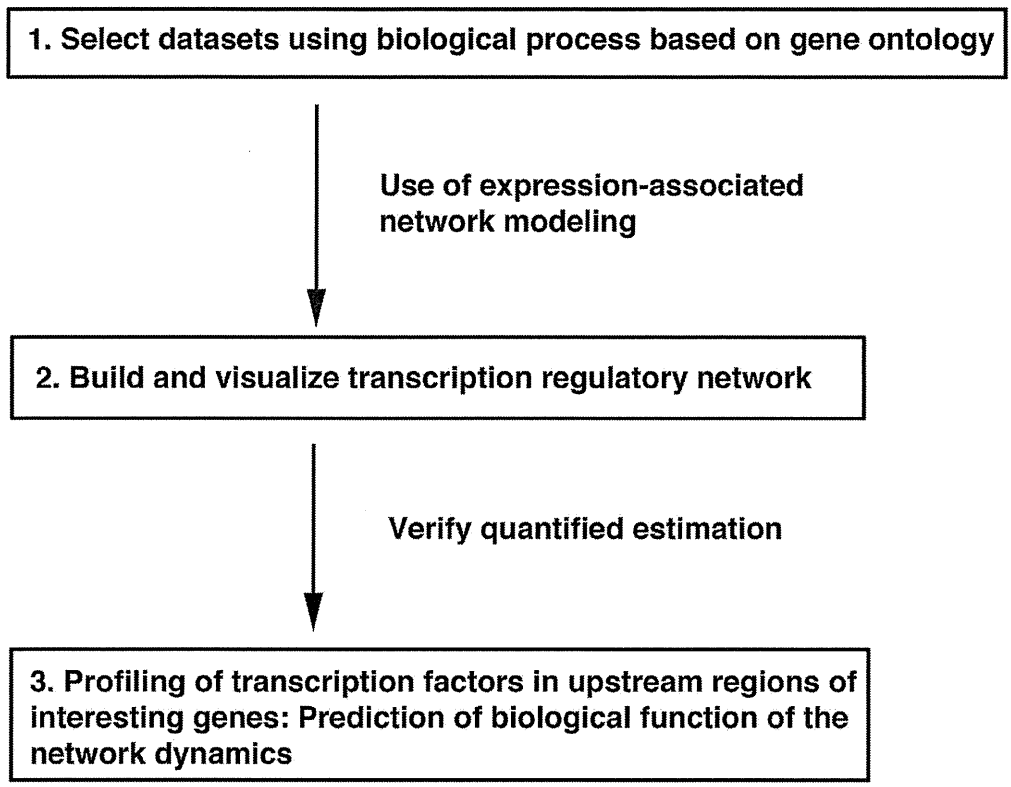

Fig. (1). Strategy used to identify, analyze, and validate regulatory gene networks.

an obvious target for this type of analysis and are the focus of our current study.

The first step in our approach was to select a data subset from a pool of genes associated with various aspects of cell cycle-related processes. The gene choices were based on the gene ontology of the mouse genome using GenMAPP, a computer application designed for the visualization of gene expression data by using maps representing biological pathways. This technique provided a qualitative tool for grouping genes (see Materials and methods). To gather gene expression data associated with the cell cycle, mouse embryo fibroblasts (MEFs) [4] were serum starved or exposed to hydroxyurea to synchronize and control their movement through the cell cycle. At various time points following the release from G0 and cell cycle re-entry, the mRNA expression levels for 6437 genes was measured using a microarray. For 10 cell-cycle related maps (Table **1**), 145 genes were measured in the microarray assay. Of these 145 genes, 50 genes met the criteria of at least 2-fold higher or lower levels as shown in Table **1**. Since the number of genes analyzed using TAO-gen had to be reduced due to computer processing limitations, 39 out of these 50 genes were finally selected for further analysis based on tissue-specific expression information and their biological significance from published articles after removing overlapping genes.

Two separate maps linking our selected 39 genes to a network were generated using the G0 course data subset (serum starvation) and the G1/S course data subset (hydroxyurea treatment). Although the expression of these genes is dynamic during the cell cycle, the networks were modeled by assuming equilibrium between the genes and by evaluating those using formal statistical methods that quantified any linkages and assessed their significance. Nodal genes (genes that appeared to be linked to a large number of other genes) were positively identified in the network. In the final verification step, the promoter regions of the genes targeted by each nodal gene were analyzed for common transcriptional factor binding sites. Finally, we discuss the roles of the central nodes and the dynamics of the quantified network in relation to the murine cell cycle.

Identification of a Gene Network Based on Expression Profiles

Representative maps using our 39 gene networks were developed separately for the G0 course (Fig. **2A**) and the G1/S course (Fig. **3A**). The number of linkages in these two networks is summarized in Table **3**. Name abbreviations of the genes analyzed in this paper are shown according to their listing in GenMAPP. These networks were developed using Bayesian networks and a mathematical model allowing each of these mRNAs to connect to any other through direct or indirect transcriptional regulation leading to gene expression changes.

The network from the G0 course data subset in which the cells had been serum starved indicates that the cyclin-dependent kinase inhibitor 2A (*Cdkn2a*) and *Cdk7* are central nodes (Fig. **2B**, **C**), whereas *E2f1*, known to regulate the G0-G1 transition, plays a lesser role. Although the *Cdkn2a* and *Cdk7* gene products and related molecules have been suggested to functions in regulating G1 entry and progression from side supportive data [26, 27], it was not clear until our current findings whether these molecules

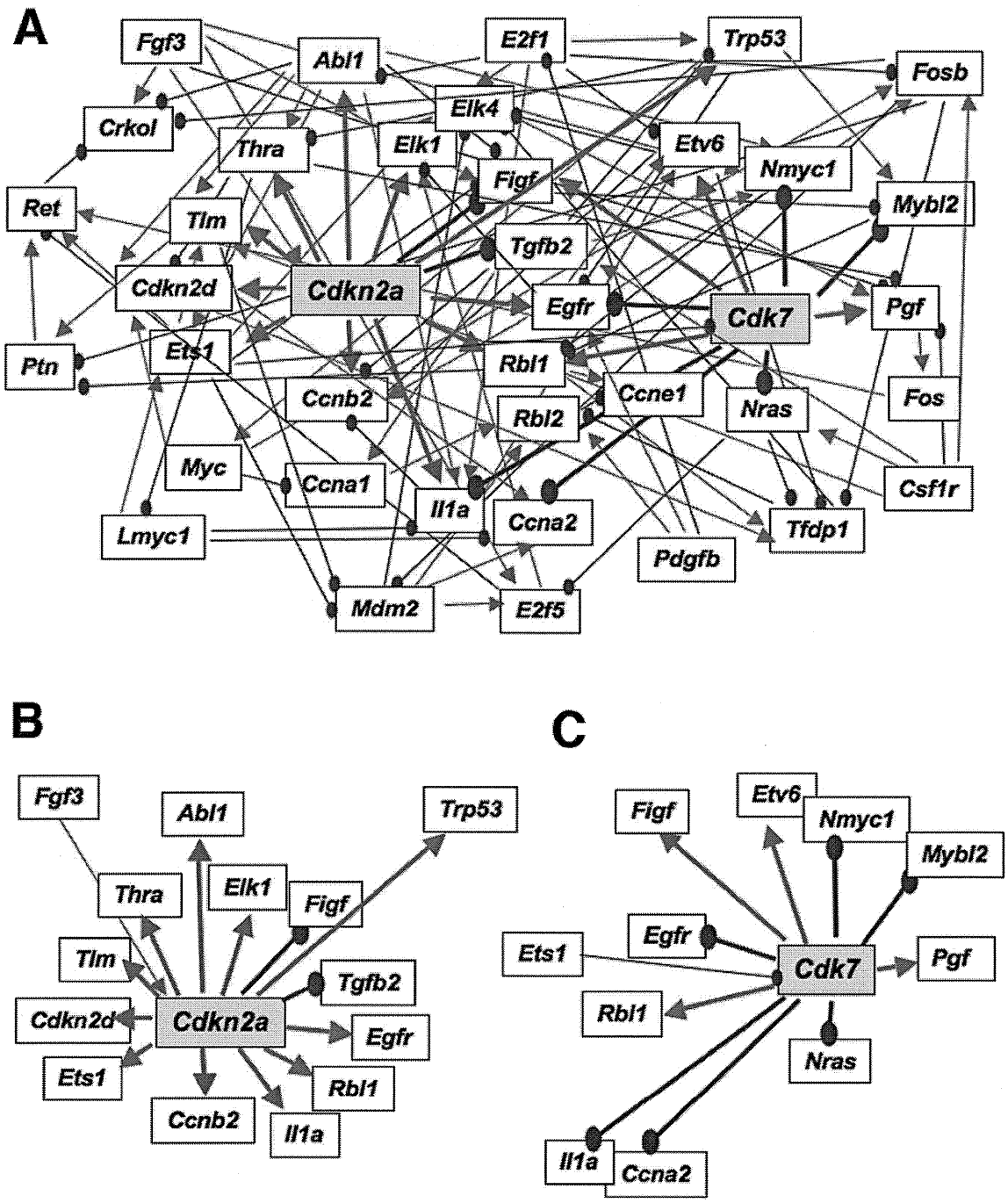

Fig. (2). Representative maps and expression graphs of the transcriptional regulatory networks for selected genes associated with cell-cycle control in MEF cells. Shown are (**A**) the network identified for the G0 course data and also the isolated linkages associated with nodal genes Cdkn2a (**B**) and Cdk7 (**C**). Bold lines indicate linkages from Cdkn2a or Cdk7 as a nodal gene. Red arrows indicate linkages associated with upregulation and blue arrows indicate linkages associated with downregulation for any two genes within the network.

functioned as central nodes in the gene networks. *Cdkn2a* and *Cdk7* were not classified as a G0 cluster *via* k-means in the first report of these microarray data [4]. CDKs are known to be key components of the core cell cycle machinery and are inhibited by cyclin-dependent protein kinase inhibitors (CDKNs). CDK7 and CDKN2A are members of the CDK and CDKN families, respectively. *Cdkn2a* also encodes $p16^{INK4a}$, a protein that indirectly regulates the activities of both pRB and p53 through the inhibition of CDK4 and CDK6. The predictive pathway from *Cdk7* suggests that CDK7 down-regulates *Ccna2*, *Egfr*, *Il1a*, *Mybl2*, *Nmyc1* and *Nras*, and up-regulates *Etv6*, *Figf*, *Pgf* and *Rbl1* (Fig. **2C**). For the time course of the expression levels *of Cdk7, Ccna2, Egfr, Mybl2, N-myc* and *Nras* following the release from serum starvation, when the cells enter G1, the expression levels of *Cdk7* are reduced, resulting in the elevated expression of *Ccna2, Egfr, Mybl2, N-myc and Nras* (data not shown).